INVESTIGATING ELECTRICAL PROPERTIES OF ADAM 3D PRINTED 17-4PH STAINLESS STEEL FOR INTEGRATED SENSING FUNCTIONALITIES

A.H. (Herjan) Barkman

BSC ASSIGNMENT

Committee:
prof. dr. ir. G.J.M. Krijnen
dr. ir. G.J.W. Wolterink
dr. ir. D. Alveringh

June, 2022

017RaM2022
Robotics and Mechatronics
EEMCS
University of Twente
P.O. Box 217
7500 AE Enschede
The Netherlands

Abstract

This study investigates integrated sensing functionalities for 3D metal printed structures using the Markforged Metal X system. The material that is printed is a polymer bonded 17-4PH stainless steel powder. A second, ceramic, material is used to separate metal parts. The printed part is washed and then sintered. The mechanical anisotropic properties of the sintered parts are found in literature. The first of three experiments looks deeper in the printing processes. The second one further investigates electrical resistivity. Finally the electrical anisotropic effects are inspected.

The washed 'brown part' is non conductive whereas the sintered part is conductive. The electrical resistivity varies, but is around the theoretical value of 98 μΩ cm with a deviation of around -5% and + 6% . Using this with the minimum printing parameters a theoretical resistor can be printed with a resistance of 122 Ω. However, stainless steel can leak through the ceramic release material and therefore electrically connecting the traxels. This gives limitations in dimensional design and the resistance that can be created. Solutions to prevent this shorting of the traxels failed during the sintering stage. Moreover, it proved difficult to accurately measure small resistances due to a varying contact resistance in the setups used. Anisotropic effects are found, but are probably not due to the structure. The resistance difference in case of anisotropy are likely too small to be of practical relevance.

Contents

List of Abbreviations

- 3D: Three-dimensional
- ABS: Acrylonitrile butadiene styrene copolymer
- AC: Alternating current
- ADAM: Atomic diffusion additive manufacturing
- BPE: Bound powder extrusion
- CB: Carbon black
- CNC: Computer numerical controlled
- DC: Direct current
- DED: Directed energy deposition
- DLP: Digital light processing
- e.g.: For example
- FDM: Fused deposition modeling
- LCR: Inductance, capacitance and resistance
- MBJ: Metal binder jetting
- MJF: Multi jet fusion
- PBF: powder bed fusion
- SLA: Stereolithography
- SLM: Selective laser melting
- SLS: Selective laser sintering
- SMU: Source measurement unit
- TPU: Thermoplastic polyurethane
- WAAM: Wire arc additive manufacturing

1 Introduction

In one year, millions of people worldwide break a bone [1]. Recovery periods of a fractured bone can take twelve weeks, sometimes even more [2]. However, estimations of the recovery time is a complex assumption in which several mechanisms have to be taken into account [2]. Therefore, a more valid procedure of making estimations has to be developed. The recovery is done using metal plates that keep the bone in the right position. It would help the doctor when these metal plates could sense how much the bone is healed. Medical implants are already made using metal 3D printers [3]. Therefore, it is interesting to know if 3D metal printing can be used to integrate this sensing into the printed structure. In this chapter an introduction to the topic is given, which leads to the research question.

1.1 Context

1.1.1 General background in 3D printing

Nowadays there are multiple 3D printing techniques. A wide variety of polymer materials can already be printed and has been researched to some extent. Schouten et al. [4] are reviewing the current state and progress of 3D printed sensors. Additionally, they explain challenges and solutions. 3D printing is a good option for small series of parts and variability in design. Polymers can be printed via several ways like Stereolithography (SLA), Selective Laser Sintering (SLS), poly jetting, binder jetting, Digital Light Processing (DLP), Multi Jet Fusion (MJF), and Fused Deposition Modeling (FDM) [5, 6].

1.1.2 Metal 3D printing techniques

Metal 3D printing already exists for a while with the first patent originating from 1980 [7]. Followed by the first direct metal laser sintering printer introduced in 1994 [7]. Now with the metal material more complex structures can be printed with respect to traditional techniques such as computer numerical controlled (CNC) fabrication, casting, molding or forging. These printed structures using the metal material are stronger than printing with composites. For example, while 3D printed continuous carbon fibre has a tensile strength of 800 MPa, printed 17-4PH stainless steel has 1050MPA. The tensile modulus are 60GPA and 140GPA respectively [8, 9]. Therefore, the metal printed structures can be used for applications where more strength is needed compared to structures printed with a composite filament.

A manufacturer of metal 3D printers is Markforged. One of the materials that can be used is 17-4PH stainless steel. The datasheet of this material compares its heat treated sintered parts with other metal production techniques [8]. Steel can be heat treated to improve its characteristics. It uses heat treated H900 specification for comparisons. Heat treated sintered parts have less strength compared to heat treated, wrought stainless steel parts. Since tensile strengths are respectively 1250 MPa and 1310 MPa while the not heat treated sintered parts have a tensile strength of 1050 MPa [8].

As there are various ways to 3D print polymers there are also various techniques for 3D metal printing. These include but are not limited to Metal Lithography, directed energy deposition (DED) via an electron or laser beam, Metal Binder Jetting (MBJ), selective laser melting (SLM), powder bed fusion using laser light (PBF), wire arc additive manufacturing (WAAM) and the traditional FDM printing with metal filament [3]. These all have their own benefits, production speed and applicable sizes. Ten different 3D metal printing techniques can be found in table 1.1. Choosing a technique is a trade-off and different techniques are best for different applications and priorities. FDM printing is specifically of interest in this research as it relates to the technique of the new 3D printer recently acquired by the University of Twente. Its ben-

Table 1.1: 10 different metal 3D printing techniques. 'Size' refers the size of the complete part. Ranging from parts being a few millimeters in size to parts being larger than a meter. XS is very small, S is small, M is medium, L is large and XL is very large. The cost is the relative cost to print a part. The detail is considered to be the minimum layer height that the printer can print. The strength is defined as the part strength. An FDM printing technique has for example a tensile strength of 1050 MPa. Adapted from [3]

Technology	Size	Cost	Detail	Strength	Max Speed
FDM/Extrusion *fused deposition* *modeling with metal filament*	S-M	$	0.05 mm	medium to high	up to 500 $mm\,s^{-1}$
SLM/PBF *selective laser melting* *or powder bed fusion with laser*	S-M	$$$	0.02 mm	high	up to 25 $cm^3\,h^{-1}$
EBM/PBF *electron beam melting or* *powder bed fusion with electron beam*	S-M	$$$$	0.07 mm	high	55 $cm^3\,h^{-1}$ to 80 $cm^3\,h^{-1}$
Metal Binder Jetting	S-M	$$$	0.035 mm	high	1500 $cm^3\,h^{-1}$
WAAM *wire arc additive manufacturing*	L-XL	$$	1 mm	high	2.2 $kg\,h^{-1}$
DED Laser *directed energy deposition* *(laser)*	M-L	$$$$	0.2 mm	high	500 $cm^3\,h^{-1}$
DED eBeam *directed energy deposition* *(electron beam)*	M-L	$$$	0.2 mm	high	2000 $cm^3\,h^{-1}$
Metal Lithography	XS-M	$$$$	0.01 mm	high	up to 300 layers per hour
Cold Spray	M-L	$$	0.38 mm	high	100 $g\,min^{-1}$
Micro 3D Printing	XS	$$$$	0.005 mm	high	–

efits, compared to the other techniques, are that it is the most cost efficient technique, while maintaining good printing speed and details in the printed parts.

1.1.3 Markforged Metal X

The metal 3D printer referred to above is the Metal X from Markforged. The FDM technique that is used is called Bound Powder Extrusion (BPE) or as Markforged calls it atomic diffusion additive manufacturing (ADAM). The material used is '17-4PH stainless steel' [8], although other metals e.g. copper and inconel 625 can also be printed. BPE is very similar to standard FDM printing, however, the filament is a mix of at least 80% metal particles binded with a polymer binder. Consequently after printing the part needs to be washed to remove most of the binder and then sintered to fuse the metal particles together [10].

Markforged has its own cloud-based slicing software called Eiger [11]. This automatically slices the STL file and adds metal support structures. It also adds ceramic material to separate the support from the part. Additionally there is an option for a raft which prevents warping of the part and makes sure it shrinks properly [10]. The slicing software also adds support structures made from stainless steel. After slicing the structure can be 3D printed.

The filament is very brittle and to prevent breaking a heating chamber is used to bring the filament at elevated temperatures. A ceramic material functions as an interface between the part and the support material. To facilitate that, after sintering, the support and the part can easily be separated.

The first step is printing the samples. After printing the samples are called 'green parts'. In the second step the samples are bathed in chemicals which dissolve most of the polymer binder. Now the sample, called 'brown part', is more fragile, but kept together with the remainder of

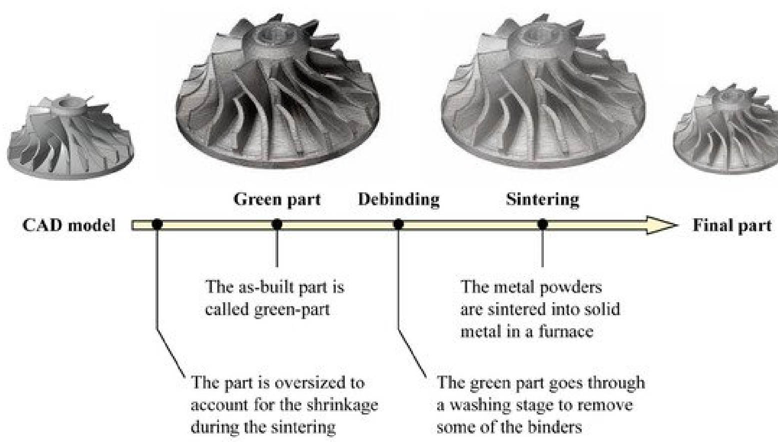

Figure 1.1: Several stages in the fabrication process of a metal 3D printed part. The sintered part is called a 'green part' and the washed part is called a 'brown part'. Adapted from [12]

the polymer binder. For the third step the 'brown part' is put in an oven which heats the part to approximately 85% of it's melting point. The metal particles are fused together, shrinking the sample by approximately 17% and burning away the remainder of the polymer binder [10]. After this the part still contains some support material, sometimes already transformed into dust. The support material is only connected via the ceramic and can be easily removed mechanically. In principle then the part is finished. Optionally the sintered sample can be sanded for a smoother surface. The part can also undergo heat treatment to improve strength, stiffness, elongation and hardness [10]. Some steps, especially washing, can take days whereas traditional production processes would take less time. Hence this way of making metal parts is less suitable for mass production. However, for prototyping or complex parts it is ideal. The complete printing process in the various steps can be seen in figure 1.1.

1.1.4 Application example

Clinic metal structures are used, e.g. to remedy fractures. However, these structures are based on experience and estimation [13]. According to Dr. F. IJpma, the more the bones heal, the more they take over the force from the plate that supports the bones around the fracture. When a patient is fully recovered, the bone has taken over the full force of the plate. This is because the bone itself heals and hence is able to endure more force [13, 14]. So, if the bone is fully recovered, little to no force will be on the metal plate. This means that the plate can be removed from the body. Currently this is only estimated by the doctors. They don't know for sure if the patient is completely recovered yet and hence advise longer recovery time than may actually be needed.

Force can be measured by a strain in the plate. A typical sensor for this is a strain gauge. Implementing a strain gauge would mean more efficient recovery as the doctors would know when the bone is fully recovered. However, external mounting sensors can be difficult. If it would be possible to integrate the sensing in the metal plate, their work can be made more accurate and efficient. An example of another kind of sensor which also measures the strain is researched by Yisong Tan et al. [14]. They use a ferromagnetic material and a magnetic sensing device to test how much tension is still on the metal plate. For these types of sensors a 3D metal printer is preferred as it is a high complex design and can be fine tuned per patient. This brings us to the problem.

1.2 Problem statement

1.2.1 integrated sensing

Nowadays it is possible to 3D print sensors. There are four aspects in which the 3D printed sensors are beneficial. The first is the versatility of the manufacturing method [4]. Additionally the freedom in complexity and customization are preferable [4]. It also saves assembly steps [4]. However, these sensors are usually thermoplastics and have strength limitations. As the sintered metal printed part is stronger, printing metal sensors can be an option.

Sensors and sensing technologies are necessary to receive information about certain structures and parts. These sensors are normally attached externally as the gained information is adequate enough. However, as mentioned in section 1.1.4, there are cases in which circumstances would not allow external mounting, or the external mounting confuses data collection and can limit gained information [15]. Integrating the sensor into the material, therefore, is reasonable. With metal 3D printing it is interesting if this sensing can directly be implemented, as the material is relatively strong and conductive.

Another research was focused on a metal 3D printed accelerometer using laser PBF [16]. They successfully made an accelerometer, however, to insulate the various metal parts insulating material was added post-production. With the Markforged BPE technique the insulating ceramic layer can be printed, so it does not need to be added post production. However, the exact material description is vague and hard to find, thus it must be investigated more. In the specific application of the fractured bone recovery example, a strong metal structure needs to sense. To current knowledge, this has not been done yet via FDM 3D metal printing. For the applications that need both a strong material, integrated sensing and must be easily customizable this is a problem yet to be researched.

1.2.2 Research question

Using the newly acquired 3D metal printer from Markforged, a strong structure with integrated sensing functionality is of high interest. However, it is most favourable when no post assembly is needed and parts can be printed as a whole. Moreover, the electrical characteristics of the material are unknown when 3D pinted using an FDM printing technique and thus should be investigated as well. That brings us to the research question:

How to make a single structure which contains integrated sensing functionality using an FDM 3D metal printer with 17-4 stainless material?

This gives challenges as to how to create isolated islands for voltage differences and other electrical sensing possibilities, like a capacitive sensing. As it is a single metal structure it is expected to be conductive and have a low resistivity. Next to that the magnetic properties can be investigated. To bring the question down into several parts for the research the following sub questions are made:

- What properties, interesting for sensing, are obtained for metal 3D printed structures?
  - Isotropic or anisotropic?
  - Resistance changes on mechanical loading?
  - Conductance changes?
  - Influence by magnetic fields?
- What are these properties for the used 17-4 Stainless steel material?
- What solutions do already exist for medical sensors and can be applied to a single metal printed structure?

- What are the quantities that need to be measured for medical applications sensors?
- How to create integrated sensing functionality?

Since the material is a metal, it is expected that the structure is highly conductive. Designs of commonly used resistors may be used for the structure to create isolated islands needed for standard electrical interfaces. The ceramic is expected to have a large electrical resistivity. However, it may be difficult to use it as it is expected to be brittle. Stainless steel in general is ferromagnetic, hence it is expected to be sensitive to magnetic fields. The printing process will be explored to get a better understanding of size and material limitations.

2 Analysis

Before developing integrated sensing structures, the material and the print limitations need to be investigated. First of all, it is known that the structure will be printed using 17-4PH stainless steel and a ceramic release layer. Therefore, the electrical and mechanical properties of these materials need to be found. Secondly, the print limitations need to be further investigated. For instance, is the ceramic release layer useful or just a byproduct and do the dimensions of the sintered parts indeed correlate with the theoretical dimensions? Afterwards several existing sensors are discussed and design ideas are evaluated.

2.1 Material

One of the two filaments the printer uses is the polymer bound 17-4PH stainless steel. The second filament is a polymer bound ceramic material. These filaments will be called the raw form of the material. After washing and sintering the polymer binder is removed. Therefore, the final part will consist of 17-4PH stainless steel and ceramic parts. 17-4PH stainless steel has many beneficial properties over other metal and composite materials. For instance, it has high tensile strength with respect to composites and high corrosion resistance up to 316 °C [17]. On the other hand ceramic is solely used as an interface between the support structure and the sample. After sintering the ceramic material is brittle and can easily be removed with a light tap of a hammer [10]. For small parts this can be problematic, since the force needed to remove the ceramic could damage the small parts as well. During sintering the ceramic material is partially burned away or turned into powder [18]. Since the material is brittle, it may be difficult to fabricate structural parts. The Eiger software gives the user the option to change all or most of the support structures into ceramic layers via its experimental mode function. Potentially allowing the ceramic to be used as isolation material. The properties of this sacrificial ceramic material are not publicly available and hence tests will be done to see if it can be used.

2.1.1 Sensing properties

There are multiple sensing technologies. A strain gauge sensor for example needs to give a substantial resistive difference when strain is incurred. This difference is defined by a mechanical strength and elongation and the electrical properties of the material itself. So to make integrated sensing functionality we not only need to look into electrical sensing properties, but also look into the mechanical properties of the materials.

2.1.2 Mechanical properties

According to the the manufacturer the elongation at break is 5% of the original length [8]. This means that the metal can stretch 5% before it breaks or tears. The ultimate tensile strength is 1050 MPa. As stated in the introduction this is 250 MPa more than the strongest composite that Markforged can 3D print, continuous carbon fibre. After heat treating the parts, the tensile strength becomes 1250 MPa. The relative density is 96%, which means it is less dense, hence lighter, but also less strong than traditionally made metals. In the introduction the heat treated sintered part was compared to a traditionally manufactured heat treated part which had an increased tensile strength of 60 MPa which is 4.8%.

The yield strength indicates the upper limit of elastic behaviour and lower limit of plastic behaviour. Below this point the deformed material will return to its initial shape. If a structure is stressed over this limit, permanent deformation will occur. This restricts the ability of the material to sustain stress. The yield strength is important for a sensor which utilizes resistance to measure strain. The 0.2% yield strength of 3D printed 17-4PH stainless steel is found to be 800 MPa [8]. The 0.2% comes from the offset that is used. Using equation 2.1 with a tensile

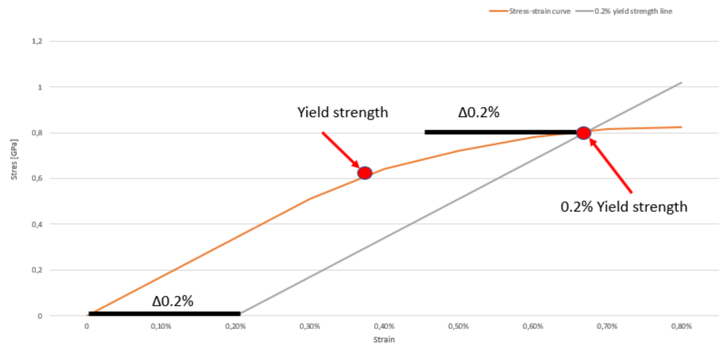

Figure 2.1: Sketch of a possible stress-strain graph using the tensile modulus of 170 GPa. The two black stripes are the 0.2% differences in strain. The two red dots show typical places for the yield and 0.2% yield strength.

modulus of 170 GPa [8] a sketch can be made. In Figure 2.1 a possible sketch can be seen. For now it assumed that the maximum strain within the elastic limit is 0.47%. This number is obtained by taking the 0.2% yield strength strain, which is 0.67%, and subtracting 0.2%. However, due to the non-linearity of stress-strain graphs, the difference in strain between yield strength and the 0.2% yield strength is in general larger than 0.2% as can also be seen in the figure. Measurements can validate the exact yield strength.

$$\epsilon = \frac{\sigma}{E} \tag{2.1}$$

2.1.3 Electrical properties

Secondly, the electrical properties will be discussed. As there is little known information about the electrical properties of printed 17-4PH the properties of the bulk material are considered. The electrical resistivity of 17-4PH is ca 98 µΩ cm [17]. This is relatively high compared to copper, which is approximately 1.7 µΩ cm [19], but also lower than Nichrome, a common material used for resistors with an electrical resistivity of approximately between 110 µΩ cm and 150 µΩ cm [19].

The bulk material is martensitic. Martensite is a crystalline structure for steel. Together with an abundant amount of iron this results in a ferromagnetic steel [20].

The printing process allows to 3D print metal without powders. However, due to printing in tracks, it imposes anisotropic effects that can occur with FDM techniques. As the printed stainless steel has a porosity of approximately 3% it is expected that the electrical resistivity has an anisotropic characteristic of the printed material. Especially because there were more voids found along the direction of printing the traces [21]. More voids and bad connections within the material can mean that the resistivity can rise as conduction is impaired.

2.1.4 Anistropic models

In the paper of Daniel Wilmes [22] the author researches a 3D-AC analytical model. The model is made to understand the electrical anisotropy of the printed material. As this paper is about thermoplastics, which do not need to be sintered, it is interesting to investigate if this still holds for the metal FDM printed product. Assumably, anisotropy would be reduced, when putting the product into the furnace, so the metal particles can fuse together.

The model is used to theoretically examine a block of stainless steel with dimensions 2.5 mm by 2.5 mm by 2.5 mm. The volume resistivity is assumed to be 98 µΩ cm. The Y and Z surface resistivity is 3.920 mΩ and 7.840 mΩ respectively. These are obtained by dividing the volume

Table 2.1: The parameters that were used in Matlab for the model of Daniel Wilmes.

Width of traxels (W)	250 µm
Height of traxels (H)	125 µm
Length of traxels (L)	1 cm
Volume resistivity (ρ)	98 µΩ cm
Surface resistivity (ρ_Y)	3.920 mΩ
Surface resistivity (ρ_Z)	7.840 mΩ
Longitudinal capacitance (C)	27.7 aF
Surface capacitance (C_Y)	88.5 nF
Surface capacitance (C_Z)	88.5 nF
Lowest frequency (F_{min})	0 Hz
Highest frequency (F_{max})	100 MHz
Number of frequencies (F_{num})	200

resistivity by the height of the correlating direction [23]. Using equation 2.2 [24] a longitudinal capacitance of 27.7 aF is calculated. Here ϵ_0 is the vacuum permittivity, H is the height, W is the width and Δx is the length. ϵ_r is the relative permittivity and in case of metals this is ≈1 [25]. The surface capacitance is then calculated by dividing by the height of the correlating direction again. In Table 2.1 the input parameters are shown.

$$C = \frac{\epsilon_0 \epsilon_r HW}{\Delta x} \tag{2.2}$$

The results can be seen in Figure 2.2. According to the model, the relative ellipsoid graph is similar to the DC example made by the author. The conductivity can be seen to be best along the X-direction which is the extrusion direction. However, it is very little conductive along the Y- or Z-direction. In the zoomed in graph in Figure 2.2b it can be seen that it is not completely zero. To conclude, according to the model an anistropic effect perpendicular to the extrusion direction in both the Y- and Z-direction is expected.

2.1.5 Investigating the print process

The printer has a heated chamber to keep the filament soft. The print sheet is vacuum-held and the printer uses auto bed leveling [10]. The printer has two nozzles, one for the metal and one for the ceramic filament. In Figure A.1 it can be seen that the width of the extrusion hole is wider for the ceramic filament release, however, details about the exact size are not provided.

The sintered material minimum part dimensions are 2 mm along the X-axis and the Y-axis. Next to that it is 1.3 mm along the Z axis. The height per layer is 0.125 mm, but 0.05 mm for the experimental version [26]. Moreover, the traxel width is 0.25 mm. The oven is the limiting factor for the final part. Post-sintered maximum dimensions are 235 mm in length, 68.3 mm in width and 69.2 mm in height although in the middle of the heating chamber a maximum height can be achieved of 80.9 mm [26].

There are several infill options. There is triangular, gyroid and solid infill. The solid infill is printed with a 45 degree angle and the next layer is 45 degree's to the left. This can be seen in Figure 3.1 at page 16 in the appendix.

Todd C. Henry et al. [21], state that the properties of produced parts show dependency on the direction of extrusion. They investigated the material's porosity and stated that this is dependent on the extrusion direction. This means that the strength along extrusion direction is larger than in the orthogonal direction. The authors suggest that the alignment of force should be carefully considered, especially through thin parts. A part with an alternating 45° angle has the

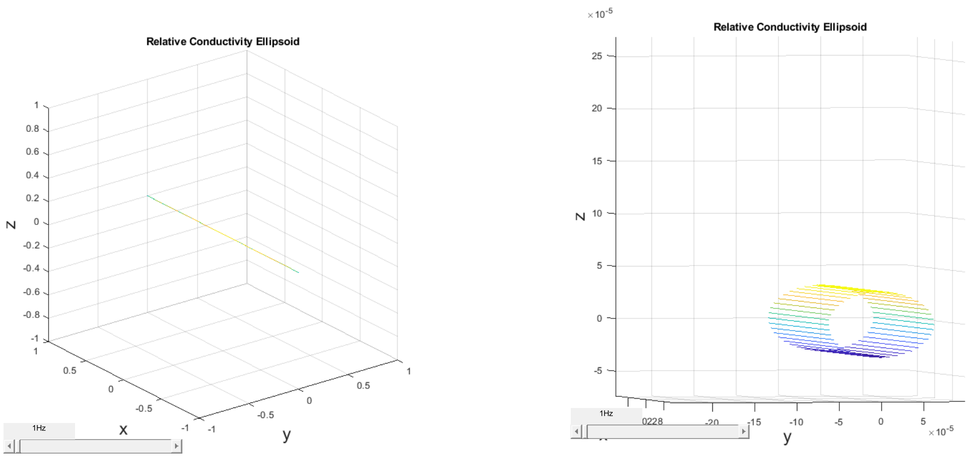

(a) A relative conductivity ellipsoid graph.

(b) A zoomed in version of the relative conductivity ellipsoid graph.

Figure 2.2: The relative conductivity ellipsoid graphs made by using the 3D model from Daniel Wilmes [22]

Table 2.2: Two different build specifications provided by the Eiger software [11]. The horizontal meandering resistor will be discussed later. The sintering time is depending on the other samples that are put in the furnace as well, however, this easily takes up a day as well.

Part	**Cube**	**Horizontal meandering resistor**
Infill	Solid infill	Triangular infill
Material	17-4PH stainless steel	17-4PH stainless steel
Printed dimensions	23.9mm x 23.9mmx23.9mm	37.7mm x 12.0mm x 6.0mm
Final dimensions	20mm x 20mm x 20mm	31.5mm x 10.0mm x 5.0mm
Print time	4h 25m	3h 9m
Wash time	3d 22h	4h
Dry time	9h 30m	1h

best mechanical multi-axial loading response [21]. So the mechanical properties are considered anisotropic. Due to this alignment of porosity's it is expected that the electrical properties are also anisotropic.

As stated earlier, the parts shrink during the sintering process. However, the exact shrinkage deviates slightly. Samples that are built with 50 µm in layer height shrink to around 72.6% of their print size while the 125 µm shrinks to around 70.1% in height while the designed dimensions were equal [12]. Therefore, the dimensions of the samples will be measured to see if they correlate with the designed dimensions.

It is possible to polish the parts. An experiment with polishing was done by Manueala Galati et al. [12]. This proved that the surface which made a contact with the raft provided the main cause of porosity while in the rest of the sample's surfaces this is close to zero [12]. That would mean that the ceramic has a negative effect on the sintering as it increases porosity's on the contact surface. Furthermore, the experiment showed that the layers are welded well together during sintering [12]. Therefore, the metal parts with solid infill are expected to conduct like a solid metal part.

The print process itself is costly in time, however, it is mainly automated and does not require human intervention. An example of printing times can be seen in Table 2.2. These times can be optimised, but it still takes a few days, depending on the availability of the person that needs to switch the samples between process phases.

2.2 Design ideas

2.2.1 Insulating material

One of the solutions for isolating different parts to create an electric potential difference would be to use insulating material. Between the two materials that are used, ceramic is expected to be insulating after sintering. However, there are a few restraints.

First of all, the ceramic is very brittle. Markforged says that with a light tap of a hammer it will pulverize if that has not already happened during sintering [10]. If the ceramic is used to insulate, that means that the design of a sensor needs to prevent too high incidental forces. It may be possible, however, to make sure the ceramic, even if transformed to dust, can not escape and hence still creates an insulating layer. It might be used as a safety switch. For example when too much force removes or breaks the ceramic and hence shorts two plates together. This could work as a mechanical fuse. Secondly, if the ceramic stays in place, the electrical properties need to be investigated because it might be useful to use it in the sensor. The test will be described in the methods section.

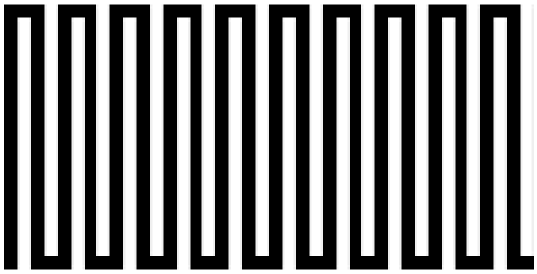

Figure 2.3: Sketch of a possible design for a meandering wire. Width of the layer is 1 cm and the length is 2 cm. The wire itself has a width of 0.5 mm.

2.2.2 Strain gauge

Another solution is to impose a voltage difference by creating resistors in the metal. First we look into the equation for resistance.

$$R = \frac{\rho l}{A} \tag{2.3}$$

Here R is the resistance, ρ is the electrical resistivity of the material, l is the length of the 'wire', A is the area of the cross-section of the wire. As the electrical resistivity was found to be 98 µΩ cm for the bulk material, it is relatively close to nichrome. Therefore, the possibility to create a resistor with 17-4PH stainless steel is promising. The exact electrical resistivity will be measured later. The printing parameters make it possible that a 'wire' of 0.125 mm height. A wire of two parallel traxels are used having a combined width of 0.5 mm. It is unknown yet if a single traxel will print without breaking and therefore, two parallel traxels should increase strength.

Now these numbers are put in an equation 2.3. This results in 0.1568 Ω for a straight wire design 10 mm. Now the wire is meandered over a layer of 2 cm in length and 1 cm in width resulting in the wire depicted in Figure 2.3. A distance of 1.95 cm can be crossed giving 19 wires of 10 mm and twenty times a small piece between the wires of 0.05 cm. This gives a total length for the wire of 20 cm.

Figure 2.3 will now be made into a three-dimensional resistor by stacking alternating layers on top of each other up to a height of 1 cm. Eighty layers fit in a height of 1 cm. However, stacking the layers directly would short circuit the wires together. To prevent this, 39 of the layers are filled with the meandering wire design. Additionally, intermediate parts are made between two layers of wire to connect them, but separate the rest of the wire. Adding the length of all these layers of wire and intermediate parts results in a total length of 782 cm. Using equation 2.3 this results in a resistance of 122.62 Ω for a volume of 2 cm^3. This means creating isolated islands is possible using these meandering resistors.

Strain gauge design

Strain gauges are sensors which sense a change in resistance due to strain. The change in resistance is measured and with that the strain can be calculated. When strain is applied to a wire, the wire gets longer, but thinner. This means that the area gets smaller and the length bigger, resulting in a higher resistance as equation 2.3 shows.

As mentioned before the yield strength limits the maximum strain and hence also the maximum change in resistance of the sensor. The difference in resistance, however, must be high enough to be able to measure. There is an equation to calculate the deviation in resistance using equation 2.4 [27].

$$\frac{\Delta R}{R_0} = \frac{\Delta \rho}{\rho_0} + \epsilon_l (1 + 2\nu) \tag{2.4}$$

Here R is the resistance, ρ is the electric resistivity, ϵ_l is the longitudinal strain and ν is the Poisson's ratio [27]. The factor $\frac{\Delta\rho}{\rho_0}$ is the piezoresistivity term and normally nonzero. However, for metals with a Poisson's ratio around 0.3 this term is equal to $\approx 0.4\epsilon_l$. [27] That means that equation 2.4 transforms into equation 2.5.

$$\frac{\Delta R}{R_0} \approx 2\epsilon_l \tag{2.5}$$

Using equation 2.3 the resistance for a wire of minimum dimensions and a length of 1 cm was calculated. This resulted in a resistance of 0.1568 Ω. For the previously assumed strain of 0.47%, a deviation of 1.473 45 mΩ can be obtained.

It must be taken into account that the alignment of forces should be considered. As stated in subsection 2.1.5 the strength is anisotropic throughout the part. That means that due to complex forms the part with integrated sensing needs to be calibrated for every unique case.

Housing

The housing of the sensor is another design aspect. The sensor should be isolated from the housing. Preferably such that the housing is electrically grounded. This can be either done with post-processing the part or by making resistors between the sensor and the housing. For simple geometric parts like a cube or beam this is possible. The aforementioned meandering resistors can be used between the various parts. However, mechanical shear and strain can become complications using these resistors. For geometrically complex parts that, for example, fit to certain unique structures this is more difficult. Future research is expected to prove this concept.

2.2.3 Magnetic sensor

For specific medical application, such as in the case of mechanical support for fractured bones, magnetic sensing is investigated [14]. In this research a material called Metglas2826 MB was used to make a bone-plate that could be used to sense the strain [14]. Measurements were performed wirelessly by using a coil, that induced a magnetic field, around the test object. The resistance of the whole structure is measured. Consequently, isolating several parts in the sample are not needed using this method.

2.3 Measuring small resistances

There are several ways to measure resistances in the range of mΩ and µΩ. Foremost it is important to eliminate any noise or offsets. As the resistance to be measured is in the mΩ and µΩ range, certain factors start playing a significant role. This section describes several considerations when measuring resistances in the mΩ and µΩ range.

The first factor that needs to be accounted for is the contact resistance. Generally there are three cases for contact resistance. Namely:

1. The contact resistance is insignificant.
2. The contact resistance is significant, but constant.

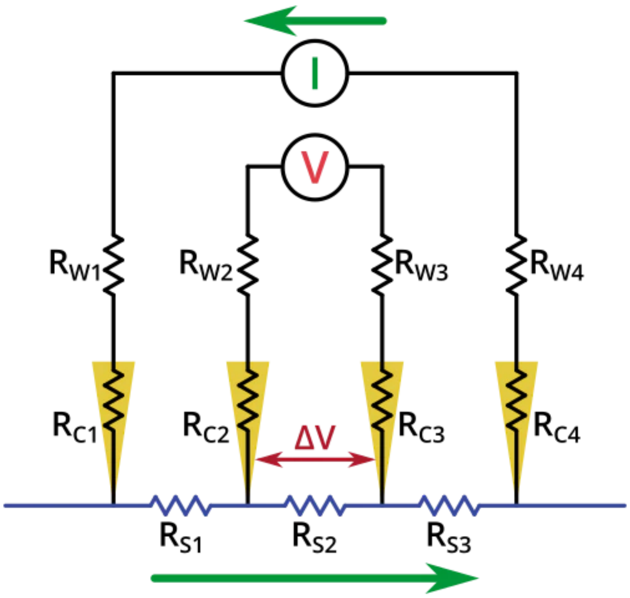

Figure 2.4: "Equivalent circuit diagram of a four-point measurement, showing the wire resistances (RW), contact resistances (RC), and sample resistances (RS). The green arrows represent current flow." Adapted from Osilla.com [28]

3. the contact resistance is significant and varies between measurements.

If the contact resistance is significant but constant, then the contact resistance can be measured and subtracted from the total measurement. When there is a significant, varying, contact resistance it will be a challenge to measure the actual material's resistance. Factors that play a role can be investigated and thus a way of making the contact resistance constant can be obtained.

To prevent measuring the contact resistance at all a four-point measurement can be done. A schematic view of this measurement method is shown in Figure 2.4. The external current source creates a potential voltage difference. This potential voltage difference can be measured using two separate probes, carrying a negligible current due to the high impedance of the volt-meter. Therefore, the voltage drop over the contact resistance is negligible during the measurement.

M. Sophocleous et al. [29] describes using sheet resistance measurements to find the electrical resistivity or resistance in general. For a thin film sample this can be useful as the equation can be simplified for the electrical resistivity. Moreover, the thin film also results in a higher resistance due to the cross-section area being smaller as can be seen in equation 2.3. For these measurements, plates with equal width and length must be printed. The equation for the electrical resistivity for this case can be seen in equation 2.6 [29]. Here, ρ is the electrical resistivity, V is the voltage, h is the thickness of the sheet and I is the current.

$$\rho = \frac{V * h}{I} \tag{2.6}$$

According to the authors, if the sample that would have been used for the sheet resistance method is damaged or printing went wrong, the Van Der Pauw technique can be used. There are five conditions that have to be met in order to use this technique [29]. These are:

- "Flat shape of uniform thickness."
- "No secluded holes."

- "Homogeneous and isotropic."
- "All four contacts must be located at the edges."
- "Contact area of any individual contact must be at least an order of magnitude smaller than the area of the entire sample."

The samples are expected to be not completely isotropic or homogeneous. Therefore, this must first be checked before the method can be of use, considering these five conditions.

Furthermore, the contacts resistance has to be lowered as much as possible in case it cannot be completely neglected using four-point measurements. For the probes it is best to use gold, because it has low contact resistance since it does not oxidise. Gold is, however, more expensive than alternatives like copper. Copper on the other hand can oxidise, which results in a higher resistance. When copper is used it must be sanded down to remove the oxidised layer.

Another problem that can arise when using dissimilar materials is thermo-electricity. Thermoelectric voltages occur when two dissimilar materials are used for circuit connections that have different temperatures. In this case a thermocouple is made for each metal to metal junction. As the samples that are being tested are also made from metal, this will probably be influential and should be taken into account during evaluation of the test results.

A possible solution for thermoelectric voltages is offset compensation. Some devices like the Agilent 34420A contain this compensation. The method of offset compensation uses two measurements. The direction of the current is reversed between the two measurements and the results are averaged. This way the thermoelectric voltage offset can be removed from the equation. This can be seen in Figure A.3 in the appendix.

Additionally, joule heating should be prevented. Equation 2.7 is derived from multiple equations and it describes the heat formed when power is dissipated in the sample. In this equation I is the current, R is the resistance, t is the time in seconds, m is the mass of the sample and k is the materials specific heat [30]. The specific heat of 17-4PH stainless steel can vary depending on the exact chemical composition and is approximately 0.460 J/g°C [17]. Dry air has a specific heat of 1.005 J/g°C [31]. Therefore, steel warms up quicker. For comparison copper has a specific heat of 0.385 J/g°C [31]. However, the sample loses heat to the environment as well. Therefore, this equation describes the worst case scenario that can be used to find the maximum thermoelectric voltage.

$$T = \frac{I^2 \cdot R \cdot t}{m \cdot k} \tag{2.7}$$

A higher current can be used to improve the resolution of the resistance measurement as the measured voltage will also increase according to Ohm's law. This is only necessary for very low resistances. With very low resistances the temperature will also not rise according to equation 2.7. Therefore, this change will be expected to be minimal with lab equipment that can measure small resistances with a small current. The Agilent 34420A is such a measurement tool. It can measure nV as well as μΩ. Table 2.3 is adapted from the user manual of the Agilent 344220A [32] and shows an example of possible thermoelectric voltages with a difference in temperature.

2.4 Conclusion

The printer can print samples using the raw forms of both the 17-4PH stainless steel and the ceramic material. After sintering the ceramic material is expected to be transformed to dust. Therefore, it might be difficult to fabricate structural parts. However, samples can be made to see if it can stay solid and therefore be used as insulating material.

Table 2.3: Table showing several thermoelectric voltages expressed in μVK^{-1}. Adapted from the user manual for the agilent 34420A [32]

Copper-to-	**Approx.** μVK^{-1}
Copper	0.3
Gold	0.5
Silver	0.5
Brass	3
Beryllium Copper	5
Aluminium	5
Kovar or Alloy 42	40
Silicon	500
Copper-oxide	1000
Cadmium-Tin solder	0.2
Tin-Lead solder	5

Mechanical and electrical properties were investigated for the bulk 17-4PH stainless steel. Elongation at break is 5% of the original length. The 0.2% yield strength is 800 MPa, which results in a strain of 0.67% with a minimal offset of 0.2% Therefore the maximum strain is considered to be 0.47%. The electrical resistivity is 98 $\mu\Omega$ cm, which is around 57 times as much as the electrical resistivity of copper. It is expected that the printed structures will have both mechanical and electrical anisotropic properties.

Meandering resistors can be printed with a resistance 122 Ω for a volume of 2 cm^3. Wires with minimum dimensions and a length of 1 cm have a resistance of 313.6 mΩ. Therefore the maximum assumed strain results in a resistance change of 2.94 mΩ.

The contact resistance can be neglected when a four-point measurement is done. Moreover, sheet resistance measurements can be done if the sample appears to be homogeneous and isotropic. This simplifies the calculation. Additionally, using a thin sample will increase the resistance measured of the sample. Offset compensation could be used to avoid measuring thermoelectric voltages.

3 Printing process

In this chapter the printing process will be examined. Therefore, conductivity of the brown and sintered samples will be investigated. Additionally, the printed dimensions of the samples will be measured to see if they correlate with the designed dimensions.

Two rounds consisting of various samples will be printed, washed and sintered. However, only the first round is described in the method and result section. The second round could not be successfully sintered and thus experiments could not be done. In the discussion the second round is elaborated more as this is meaningful for the next two chapters and for future research.

3.1 Methods

3.1.1 Samples

The first set of samples is intended to see how the dimensions after sintering differ from the designed dimensions. It contains four cubes. The detailed information of the samples is noted in Table 3.1. 'SC' properties mean that the cubes are printed with a layer height of 0.125 mm, contain a raft and have solid infill as shown in Figure 3.1 with the default option of four wall layers. The designs are made using Solidworks [33]. Furthermore, the samples are sliced using the property settings in the Eiger software [11].

3.1.2 Measurement setup and protocol

Using a Fluke 179 multimeter a two-point resistance measurement is done on samples C1 and C2. The probes are first placed on opposite edges on the top surface of the cube. Afterwards, the probes are moved inward towards each other until the two probes touch in the middle. By moving the probes inward on sample C1 and C2, the measured area decreases. Because of this, the smaller samples C3 and C4 will not be measured. These measurements are performed after the washing stage and after the sintering stage.

Dimensions are measured using an electronic digital caliper from RS [34]. By using a microscope the surface of the four printed samples can be seen in more detail. Therefore, variations between the several faces can be inspected.

3.2 Results

3.2.1 Electrical properties of brown and sintered parts

The results using the Fluke 179 proved the brown parts to be non-conductive for both C1 and C2. However, samples C1 and C2 are conductive after sintering. Additionally, samples C3 and C4 were measured after sintering for verification and proved to be conductive as well. In Figure 3.2 a measurement on the brown part sample C1 can be seen.

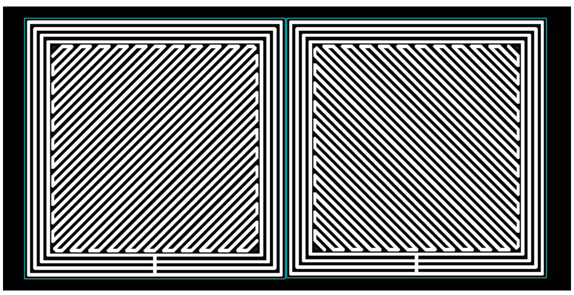

Figure 3.1: A 2D view of the 1 cm^3 cube. Here two consecutive layers are shown. Left is a layer with a 45° angle to the right and right is a layer with a 45° angle to the left as seen from the bottom.

Table 3.1: Table containing information of the samples of the first round. SC means the sample has Solid infill, 17-4PH stainless steel, 0.125 mm layer height, four wall layers and contains a raft.

Name	Dimensions	Properties	Form
C1	8 cm^3	SC	Cube
C2	8 cm^3	SC	Cube
C3	1 cm^3	SC	Cube
C4	1 cm^3	SC	Cube

Figure 3.2: The brown part sample C1 being measured. A resistance measurement with the Fluke 179 multimeter is made, but as can be seen the result of the device is OL which means open-circuit.

3.2.2 Dimensions

The samples were printed with several imperfections on the surfaces. After the washing stage these imperfections were no longer visible and the part was smooth. Pictures of the samples can be seen in the appendix Figure A.2. The dimensions of the cube samples were all larger than designed, ranging from 0.5% more in the width for sample C1 to a maximum of 4.1% more for the height of sample C3.

3.3 Discussion

3.3.1 Conduction

Markforged states that the brown part contains open canals where the binder was before [10]. So the metal particles may not all be in contact to enable electrical conduction. Therefore, only after sintering the sample and fusing the particles together the steel is electrically conductive. The green part was not measured on conductivity, although it could be interesting to measure this in future research as the conductive properties could change when the polymer binder is still completely in the part.

The furnace has an automated program for sintering. However, it could be interesting to change the settings such that the metal particles in a sample do not completely fuse. For example the time that a sample is in the furnace could be lowered. Therefore, fusing the metal particles on the surface of the sample, but not the inner part. Consequently, the inner part could be used as an insulator. For that purpose, the different conductive properties of the brown and sintered part could be used.

3.3.2 Leakage

After sintering the ceramic was pulverized, as expected based on prior research. However, it was not known beforehand that stainless steel droplets could leak through the ceramic release layer. The leakage is demonstrated in Figure 3.3. A measurement showed that the cube and the raft were shorted with a contact resistance below 1 mΩ.

3.3.3 Second printing round

Another build was made, but could not be sintered successfully. However, some pieces of this round could be salvaged for further experiments described in chapter 4 and 5. The build for the second round consisted of ten separate samples made of 17-4PH stainless steel. Eight samples

(a) A microscopic top view of sample C3.

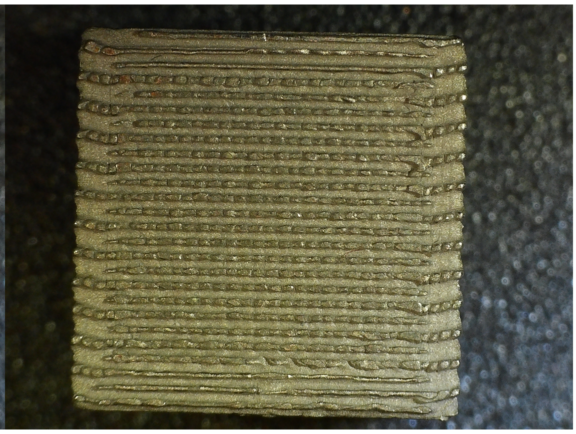

(b) A microscopic bottom view of sample C3.

Figure 3.3: Two pictures taken by a microscope of the top and bottom of a metal printed cube. The bottom has some leaked metal lines, while the top is smooth.

Table 3.2: Table containing the detailed information of the samples of the second round. SM means the sample has triangular infill, 17-4PH stainless steel, 0.125 mm layer height, four wall/roof/floor layers and contain a raft.

Name	**Dimensions** **[LxWxH]** [mm]	**Properties**	**Form**
R1	31.5x10x5	SM	Resistor, 1-layer
R2	31.5x10x5	SM	Resistor, 1-layer
R3	31.5x10x5	SM	Resistor, 3-layers, each separated by one layer of ceramic
R4	31.5x10x5	SM	Resistor, 3-layers, each separated by one layer of ceramic
R5	31.5x10x5	SM	Resistor, 3-layers, each separated by four layers of ceramic
R6	31.5x10x5	SM	Resistor, 3-layers, each separated by four layers of ceramic
H1	31.5x10x5	SM	Resistor, 0.5 mm diameter wire printed horizontally.
V1	31.5x5x10	SM	Resistor, 0.5 mm diameter wire printed vertically.
P1	10.5x10x10	SM	Four wires of 1 cm length and diameter of 0.5 mm. A 1 cm^2 plate with thickness 0.5 mm.
P2	5x5x3.5	SM	Three 0.25 cm^2 plates of thickness 0.5 mm separated by ceramic

were resistors with interface pillars. Additionally, two samples consisted of several separate wires and plates. In Table 3.2 the detailed information of these samples can be seen. 'SM' properties consist of a layer height of 0.125 mm and a triangular infill with default four layers for roof/floor and wall layers. They also contain a raft. In Figure 3.4 the total build can be seen.

These samples are made using the Experimental Alpha mode in Eiger. The automatically added 17-4PH stainless steel support is changed to ceramic release layer. As was found after the first printing round, stainless steel leaks through the ceramic. Therefore, to prevent leakage, the resistors were connected at the top of the interface pillars.

The sintered samples of the second round can be seen in Figure 3.6. Sample V1 was a meandering resistor, but printed vertically so that the meandering wires would turn into pillars. In Figure 3.5 the sample can be seen as shown in the slicer software. During the second printing process the pillars of sample V1 showed stringing, without printing the pillars, which made the sample unusable. The stringing was successfully sintered, this proves that a piece with a width and height of one traxel can be sintered as well.

Furthermore, the meandering resistor with three layers with one layer in between was printed. However, the one layer in between was meant to be filled with ceramic, but it was not seen beforehand that the slicer software did not do that. This was mistakenly done and proved indeed

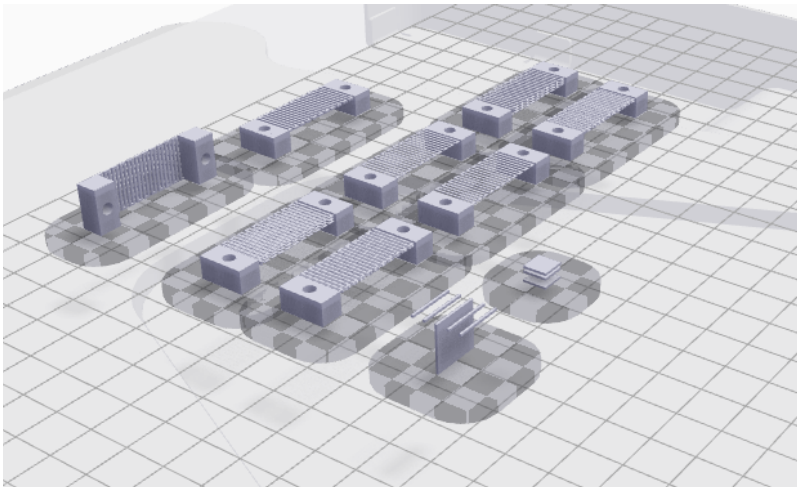

Figure 3.4: The total build of round two. The checkerboard is the raft. Left top the two samples for vertical and horizontal meandering resistors can be seen. In the middle three pairs of different meandering resistor designs can be seen. In the right bottom two samples with plates and wires are shown. (Screenshot from Eiger.io [11])

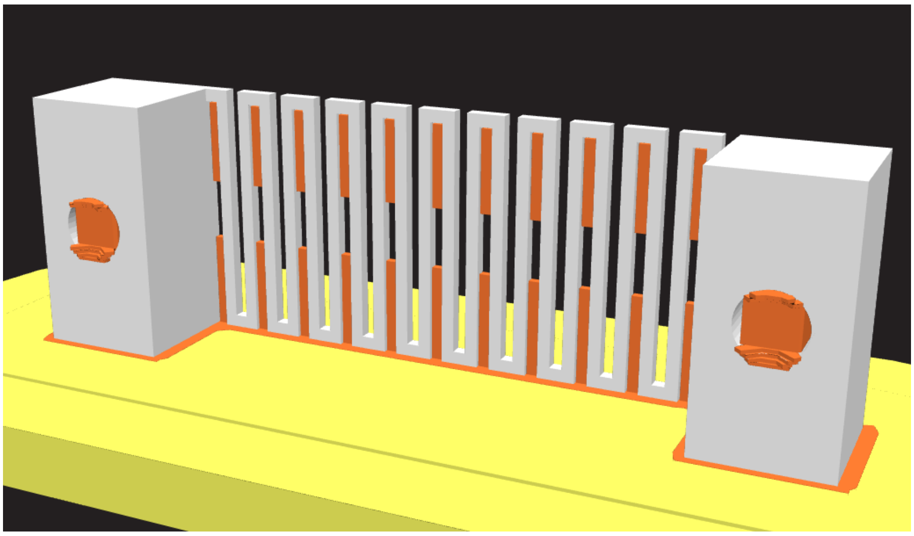

Figure 3.5: The meandering resistor printed vertically. Screenshot from Eiger.io [11]

Figure 3.6: A picture of the second round of samples made after sintering.

to be unsuccessful, because the layers fell on top of each other and thus making a wire with a three layer height.

3.3.4 Recovered samples

The stainless steel support layers of all the samples were replaced by the ceramic material. During the sintering process this proved to be too fragile. The result can be seen in Figure 3.6. The samples, but also the raft contain cracks. The ceramic dust is partially combined with the metal and turned hard. The samples H1, R3 and R4 sank into the ceramic, but were partially intact.

Most of the samples broke during fabrication. It is thus not completely clear how feasible it is to print with very small dimensions and still being able to separate the ceramic from the metal. Because of the cracks in the failed fabrication round it is expected that also the stresses that are caused by the high temperature in the furnace define the success of the sintering process.

Parts of the samples that could be recovered from the failed samples are shown in Table 3.3 with the accompanying detailed properties. Examples of these salvaged parts can be seen in Figure A.5 in the appendix. These parts will be used to do measurements in chapter 4 and 5.

The samples W5 and W6 are salvaged from the meandering of three single layers above each other without the ceramic in between. Without the ceramic in between they were fused together during the printing process, meaning they were approximately 0.375 mm thick. They could be salvaged as the wires were relatively thick, just like the meandering samples could be salvaged from the 0.5 mm thick meandering resistor.

3.3.5 Dimensions

The sintered salvaged samples contained little pieces attached to them making it sometimes up to 0.67 mm in diameter instead of 0.5 mm. The printer makes sometimes a small mistake or is inaccurate in printing dimensions. This influences the geometry and hence makes the resistivity measurements less accurate.

3.4 Conclusion

Two printing rounds were made, revealing variations in dimensions of the samples. The largest difference was measured to be 0.41 mm in the height of sample C3, which is 4.1% more than the initial height of 1 cm. Additionally it was found that the samples are only conductive after the sintering phase.

The replacement of all metal support structures proved to be too fragile. Therefore, the sintering of these samples failed. However, some parts of the samples could be salvaged.

Table 3.3: A list of the recovered samples. The dimensions are given in total length L and diameter D of the wire.

Name	**Dimensions** [L **x** D] [mm]	**Salvaged from sample**	**Form**
W1	10x0.5	H1	Wire
W2	10x0.5	H1	Wire
W3	10x0.5	H1	Wire
W4	10x0.5	H1	Wire
W5	10x0.375	R3	Wire
W6	10x0.375	R3	Wire
M1	20x0.5	H1	Meandering wire
M2	20x0.5	H1	Meandering wire
M3	25x0.5	H1	Meandering wire

4 Experiments on the resistance

In this chapter the electrical resistivity of the 17-4PH stainless steel is investigated. Therefore, resistance measurements are done in two experiments. Various salvaged samples are used for this and the results are compared and discussed.

4.1 Methods

4.1.1 Samples

The electrical resistivity will be measured. For this purpose the salvaged samples of Table 3.3 are used. The dimensions and forms are given in the same table.

Experiment one

For the first experiment the salvaged 'wire' samples W2, W3, W4, W5 and W6 are used. Together with the 'meandering' samples M2 and M3. Multiple samples are chosen to validate the measurements.

The resistance should scale linearly with the length and therefore, result in the same electrical resistivity regardless of dimensions. This only holds for the wire samples as the cross-section is expected to be equal along the wire. To validate the printer's repeatability, the longer meandering wires are measured. However, the meandering samples have corners, which are expected to give a constant deviation per corner in the measured resistance.

Experiment two

Measurements will be performed on sample W1 and sample M1. Sample W1 has a length of 1.05 cm and an approximate diameter of 0.5 mm. M1 contains two long parallel parts, the legs, of which one has a length of 8.24 mm and the other a length of 8.33 mm. They are connected with a 0.61 mm part in between on one end.

4.1.2 Measurement setups

Experiment one

The lengths of the samples are different due to the salvaging. So, first the length of the samples will be measured using an electronic digital caliper from RS [34].

Samples are tested according to the setup displayed in Figure 4.1. The Agilent 34420A can function as a nanovoltmeter or as a micro-ohm meter [32]. For this setup, the Agilent combined with its four-point resistance measurement is used as a micro-ohm meter.

The setup includes a standard in which two copper plates are built in. These are pulled together using two springs. The Agilent has two channels. For a four-point measurement both channels are used. In this case, channel one acts as a current source. The copper plates have holes tapped on both ends. Screws clamp the wires of channel one onto the copper plates. Channel two is attached to two gold coated pogo pins which are used to measure the voltage. The two voltage measuring probes are placed by hand on the outer ends of the sample. The pointy ends, make sure the contact is more precisely determined. The pogo pins also have a spring, damping vibrations from the hand during measurements. The micro-ohm meter is set on the most sensitive range. This means that the current is automatically set to 10 mA by the device [32].

The tests are verified using the HM8118 LCR meter (Rohde and Schwarz [35]). The cables of the LCR were attached using gold covered crocodile beak clips on both ends of the samples. The LCR meter has a resistance range of 0.01 mΩ to 100 MΩ with a deviation of ±0.05% on the

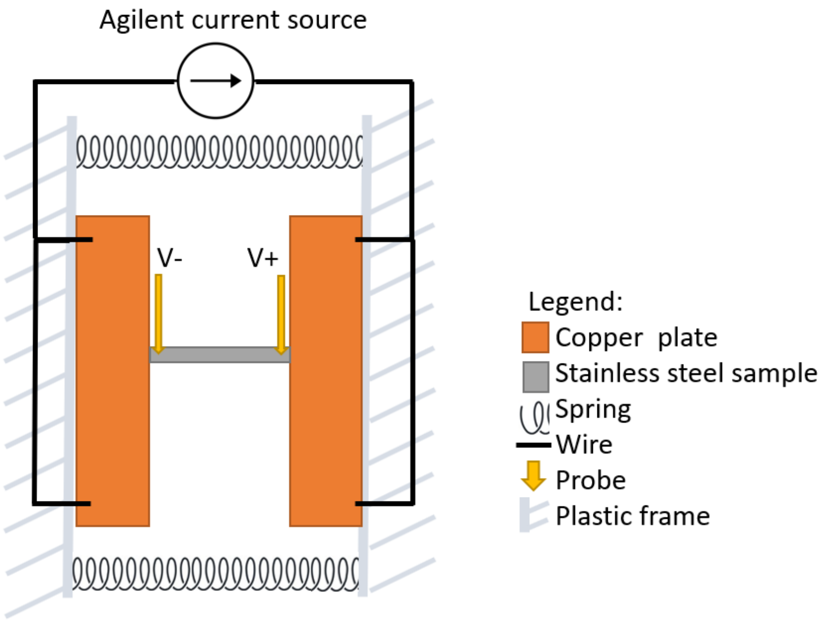

Figure 4.1: A schematic top view of the test setup with the copper plates.

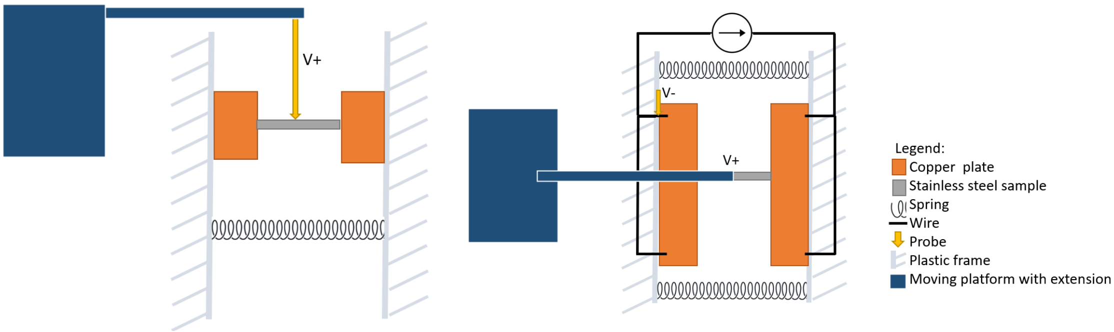

(a) A schematic side view of the setup. **(b)** A schematic top view of the setup for experiment two.

Figure 4.2: A schematic side and top view of the test setup for experiment two. The $V-$ probe is attached on the outside of the copper plate. Therefore, the contact resistance on one side is measured as well.

measured value [35]. It also uses a four-point measurement, therefore correcting for contact resistance.

Experiment two

A setup that can accurately move over distance and measure the resistance is displayed in Figure 4.2. For this the test setup containing the copper plates of the setup from Experiment one is extended with a moving platform. This platform consists of three blocks that can each be moved into one of the XYZ-directions. The blocks are moved using precision screws with a resolution of 100 µm. The accuracy is dependent on the user as the precision screws are operated manually.

The current source is connected to the copper plates using the screws. The $V-$ probe is now clamped with the screw to the copper plate as well instead of being held by hand. Therefore the contact resistance between the sample and the copper plate where the $V-$ probe is situated will be measured as well. The $V+$ probe is attached to an extension of the moving platform.

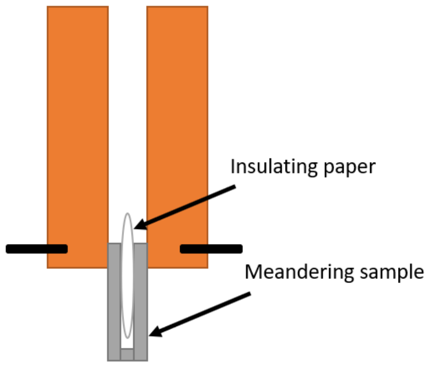

Figure 4.3: A close up schematic view of the meandering sample M1 in the test setup of 4.2. Samples M2 and M3 were put in the test setup the same way.

4.1.3 Measurement protocol

Experiment one

In Matlab the Agilent is controlled and the data is processed. The measuring probes are put on the opposite far ends of the sample by hand. The software from appendix A.6 is used and 25 measurements are done. Additionally, thermoelectric voltage offset compensation is used and every measurement is averaged over twenty measurement cycles. The mean and standard deviation are found using Matlab.

Sample W3 is used twice, the second time, however, after every measurement the sample is removed and then placed in the set-up again. This is done to see how much the positioning influences the measurements by repeatedly placing the sample between the copper plates. This second measurement method on sample W3 is called 'W3 (trigger)'.

Experiment two

For the second experiment Matlab will be used again to control the Agilent and process the data.

The samples are placed between the copper plates once. The moving platform is used to move the $V+$ probe over the sample. It can be moved in three directions, respectively along the X, Y and Z-directions. Every time it is moved a measurement is triggered using Matlab. The first five measurements will be 100 µm apart. Then three measurements with steps of 200 µm and two of 300 µm will be done. Therefore, it can be seen if the resistance scales linearly over parts with different lengths. From the tenth measurement on a measurement is taken every 500 µm until the end of the sample.

In case of the meandering samples a piece of thin isolation material, folded paper, was used between the meandering lines. Otherwise the wires would short circuit and the length would not correlate with the resistance anymore. A schematic view of a meandering sample in the setup can be seen in Figure 4.3.

In Matlab a least mean square fitting will be used to analyze the measurements. This results in a linear model containing an offset and a linear variable. The offset is the contact resistance at the start whereas the linear variable is the electrical resistivity.

Table 4.1: Samples were measured in length before the resistance measurements were done. The values are an average and the standard deviation of these are behind the ± sign

Part	**Length** [mm]	**Resistance** [Ω]	**Resistance with contact resistance** [Ω]	**Verification with LCR** [Ω]
W2	10.37	0.0518 ± 0.0005	0.1301 ± 0.0026	0.0418
W3	10.50	0.0496 ± 0.0085	0.0943 ± 0.0003	0.0399
W3 (trigger)	10.50	0.0456 ± 0.0112	0.0766 ± 0.0003	0.0399
W4	10.05	0.0513 ± 0.0117	0.1258 ± 0.0024	0.0392
W5	9.05	0.0669 ± 0.0048	0.1172 ± 0.0031	0.0531
W6	9.68	x	x	0.0567
M2	19.90+0.63	0.1233 ± 0.0027	0.1345 ± 0.0055	x
M3	9.84+10.36+5.15	0.1687 ± 0.0292	0.2089 ± 0.267	0.096

Table 4.2: The results of the measured resistances next to the measured verification resistance and theoretical resistance.

Part	**Resistance** [Ω]	**Verification with LCR** [Ω]	**Theoretical resistance** [Ω]
W2	0.0518	0.0418	0.0407
W3	0.0496	0.0399	0.0412
W3 (trigger)	0.0456	0.0399	0.0412
W4	0.0513	0.0392	0.0394
W5	0.0669	0.0531	0.0473
W6	x	0.0567	0.0506
M2	0.1233	x	0.0805
M3	0.1687	0.0960	0.0994

4.2 Results

4.2.1 Experiment one

Table 4.1 shows the significance of the contact resistance. For the first wire it is 1.5 times the measured resistance without the contact resistance. Samples W3 and W3 (trigger) are the same, but the measurement protocol is different. After every measurement sample W3 (trigger) is built in and out again as stated in the methods. The standard deviation is 3 mΩ larger, but the contact resistance was half as large. It is noticeable that the contact resistance of M2 is relatively small compared to the others with 10 mΩ to a resistance of 123.3 mΩ. The standard deviation of sample M3 is 29.2 mΩ, which is noticeably higher compared to the others.

The measured resistances using the LCR are given in table 4.2. It can be seen that they are around 10 mΩ or 20% lower than those measured with the setup using the Agilent. The electrical resistivity of the printed material is varying among the samples between 94 µΩ cm and 166 µΩ cm.

The resistance of the samples W5 and W6 are here higher than the samples W2, W3 and W4. Which is a consequence of the difference in thickness. Samples M2 and M3 that were measured with the Agilent were respectively 43 mΩ and 73 mΩ higher than the measurements using the LCR. M2 could not be measured by the LCR meter as one of the legs broke off during testing. Using the LCR, the resistance of M3 was 3.5% lower than the theoretical value.

4.2.2 Experiment two

In Figure 4.4a the results can be seen for experiment two. Here the red circles are the measured data. Moreover, a linear blue line can be seen, which is the least mean square curve fit. The linear variable is 4.16 $\mathrm{m\Omega\,mm^{-1}}$. This would give an electrical resistivity of 104 µΩ cm, which

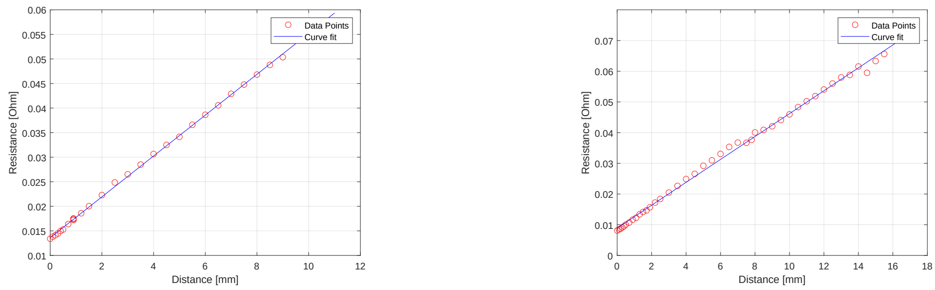

(a) The results of the resistance over length measurements of the wire.

(b) The results of the resistance over length measurements of the meander.

Figure 4.4: The results of the resistance over length measurements. The red circles are the measurements, the blue line is the least mean square fitted curve.

is 6.1% more than the theoretical value. A value of 13.6 mΩ created by contact resistance on one of the ends of the wire was also found. The code for the least mean squares method can be found in appendix A.7.

The total contact resistances of sample W1 was measured twice. One measurement being 32 mΩ and the other 41 mΩ for the total contact resistance. The standard deviation in Table 4.1 had a maximum of 3.1 mΩ for similar samples.

The curve fitting and measurement points of sample M1 can be found in Figure 4.4b. The total length of the wire was measured to be 1.8 cm. The linear model for this sample proved to be 3.72 mΩ mm^{-1} with an offset of 8.97 mΩ. This would give an electrical resistivity of 93 µΩ cm, which is 5.1% lower than the theoretical value for the bulk material. The difference between the measurements per 100 µm had a mean of 372 µΩ and a standard deviation of 108 µΩ. The offsets were not taken into account with these calculations.

4.3 Discussion

4.3.1 Experiment one

The recovered samples were tested according to the test setup made for the cubes and shown in Figure 4.1. It was found that the Agilent has a time-delay before starting the measurement. Every time a measurement was done the first four results gave an open-circuit resistance of 9.9×10^{37} Ω. Therefore, only after deleting these four, the mean and the standard deviation were calculated.

The crocodile beaks of the LCR are more wide than the sharp ends of the pogo pins. This means that the length of the wire in some cases is approximately one millimeter smaller. One millimeter makes a difference of 3.9 mΩ. In the worst case this could be two millimeter less length as there is one beak on both sides. Resulting in a resistance difference of 7.8 mΩ. However, this mistake with shortening the sample test length could also happen by hand when the samples were measured between the copper plates. Therefore experiment two was needed to verify this.

4.3.2 Experiment two

The resistance of sample W1 was 6 μΩ higher, while sample M1 was 5 μΩ lower than the expected theoretical resistivity. When looking at the curve fitted plots in Figure 4.4a and 4.4b it can be seen that data plots fluctuate around the linear blue line. The standard deviation between measurements over 100 μm was 108 μΩ which is 29% of the mean. Hence, even when measuring over small distances of the same sample fluctuations in electrical resistivity could be found. It may be that the unsuccessful sintering caused these fluctuations in electrical resistivity. In that last case it could be noticed that some salvaged samples were more fragile than others. This could mean that the different traces did not completely fuse together resulting in a higher electrical resistivity. Hence, accurate results are difficult to obtain using these salvaged samples.

4.3.3 Electrical resistivity

The measurements for both experiments gave very different results. First of all while measuring the samples in experiment one, the results showed to be 10 mΩ higher than the theoretical and LCR measurements. Sample W1 in experiment two showed that the resistance of the whole sample had the same resistance as the samples W2, W3 and W4 using the Agilent. The difference however, is that with W1 it can be seen that there is a 13 mΩ offset. When subtracting that offset the results of the resistance of the wire itself are similar to those of the LCR meter and theoretical values. Therefore it can be assumed that the electrical resistivity is indeed around 100 μΩ cm.

4.4 Conclusion

Measurements were done on salvaged samples to see how the resistance behaved. Additionally, the electrical resistivity that was found in experiment 2 showed that the electrical resistivity deviated approximately ±5-6% around the theoretical electrical resistivity of 98 μΩ cm. The samples were measured using different setups. The significant differences in results showed the challenge of measuring the small resistances accurately. Next to that it showed that printing these small wires is sensitive to fluctuations in dimensions. For a more trustworthy sensor bigger wires can be made to minimize the effect of these fluctuations on the resistance at the cost of even smaller resistances.

The setup described in Figure 4.1 showed larger differences compared to measurements using the LCR meter. The salvaged samples were not equal in strength and hence, some were more fragile than others. This can mean that the sintering of the samples was not the same due to the failed sintering process. In that case the samples are unusable for accurate measurements due to the change in resistance or even electrical resistivity and further research is needed.

5 Experiments on anisotropy

Next to the electrical resistivity, the anisotropy of the material will be investigated. As the samples of the second printing round did not successfully sinter, resistance measurements will be done only on the cubic samples of round one. First the setup is described. Afterwards the results will are given and discussed resulting in a conclusion about the electrical anisotropic properties.

5.1 Methods

5.1.1 Samples

The cubic samples from Table 3.1 will be used. Using equation 2.3 an expected resistance of 98 μΩ for the C3 and C4 cubes is found. Similarly, for sample C1 and C2 the resistance is expected to be 49 μΩ. The resistances are expected to be the same for the samples with same dimensions. Therefore, measurements on sample C1 will be verified with C2. Correspondingly, C3 will be verified with C4.

5.1.2 Measurement setup

The same setup that was discussed in chapter 4 is used. However, the setup is adjusted to make it suitable for the cubic samples. Two different configurations will be used. The first is the Agilent 34420A combined with its four-point resistance measurement [32]. The second is an external current source in combination with the nanovoltmeter of the Agilent 34420A.

An external current source and the first channel of the Agilent 34420A are attached to the copper plate via the screws. The external current source is made by limiting the current on the Skytronic 650.683 DC supply [36]. The Agilent 34420A is chosen as it has a resolution of 0.1 μΩ [32]. A tightening screw is holding the two plastic frame parts together. Two straps of double sided tape attach the copper plates to the plastic frame of the standard, preventing the copper plates from getting loose or resting on the metal tightening screw. The complete setup can be seen in Figure 5.1.

The nanovoltmeter is used to measure the voltage between the two copper plates and thus the voltage drop over the sample that is clamped in between. Channel one is utilised for this. Before this is done, the micro-ohm meter with four-point measurement is used as verification to illustrate the total resistance.

The cubes are relatively compared to the wires large and hence it is not completely known how the current will flow through the samples. Therefore, the whole surface of the cubes should contact the copper plates to divide the current equally throughout the sample. The surfaces of the samples are not completely smooth. Therefore, a thin square of copper wool is added on both sides between the sample and the copper plate. The probes, however, cannot be put on top of the sample. Therefore, the wires are connected such that a two-point measurement is done and thus measuring the contact resistance of the copper wool.

The complete setup can be seen in Figure 5.1 where the current source is external and the voltage measurement nodes are connected to the current wires.

The setup does not give any insights if the resistance measurements vary disproportionately. A maximum variation of 10% between the same cubes over the same direction will be used before the measurement setup becomes unusable.

5.1.3 Measurement protocol

For clarity Figure 5.3 is added to see how the measurement directions are defined.

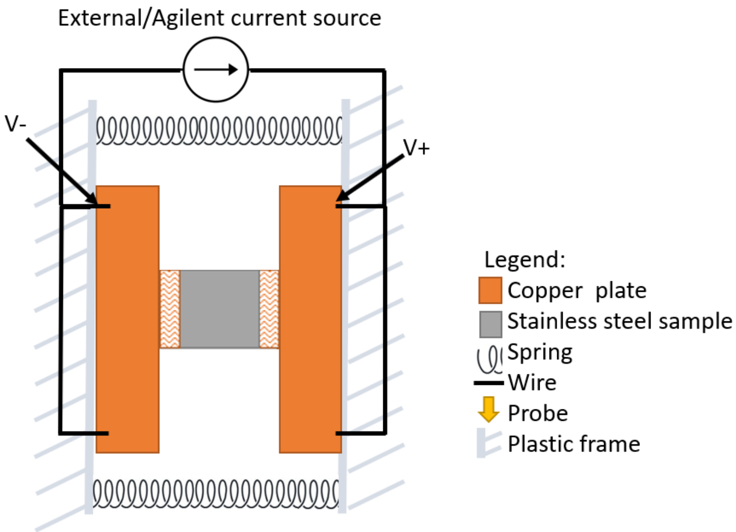

Figure 5.1: The test setup for measuring the cubic samples on anisotropy. Due to the way the wires are connected a two-point measurement is done.

An IV curve will be made, using an increasing current from the external current source. The accuracy of the constant current (CC) function of the external current source is 10 mA [36].Hence, measurements will be done with the minimal steps of 10 mA. Constant current means that the load requires more current than the current limit. Therefore, the current limit is acting as a current source, while the voltage can vary.

For the first measurement a total of twenty readings will be done to see if the IV curve is indeed a linear function. The first measurement will be verified by using the micro-ohm meter configuration and connecting the wires like the previous setup of chapter 4 shown in Figure 4.1.

Five measurements are done for the other directions of the sample. This is done with respectively a current of 0.01 A, 0.05 A, 0.1 A, 0.15 A and 0.20 A.

5.2 Results

5.2.1 IV curve of the cubes

The cubes were tested and with the external current source an IV curve is taken. The resulting plot can be seen in Figure 5.2. As can be seen for currents up to 200 mA the sample behaves linearly.

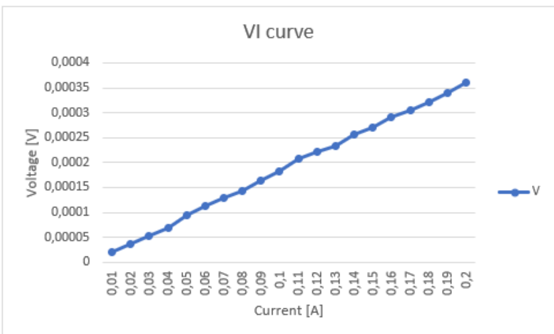

Figure 5.2: A graph plotting the voltage over a 8 cm^3 cube to an increasing current.

Table 5.1: The results of the resistance measurements along different directions of the various cubes. The measurements with the micro-ohm meter are made only once, therefore no standard deviation is shown. The results in the right column are the mean and the standard deviation.

Sample	**Direction**	**Resistance measured with the micro-ohm meter** [mΩ]	**Resistance measured with the external current source.** [mΩ]
C1	$Y+$	1.3	1.82 ± 0.08
C1	$X+$	1.3	1.47 ± 0.27
C1	$Z+$	1.0	0.96 ± 0.06
C1	$Z+$, but turned 90°	0.8	0.87 ± 0.12
C1	$Y-$	1.6	1.35 ± 0.13
C1	$X-$	1.7	1.77 ± 0.16
C1	$Z-$	0.96	0.99 ± 0.04
C3	$X+$	1.3	1.4 ± 0.06
C3	$Z+$	1.0	1.03 ± 0.03
C2	$X-$	1.7	1.77 ± 0.03
C2	$Z-$	0.6	0.67 ± 0.03

5.2.2 Anisotropy

The cubic samples were tested on anisotropy. The result of these tests can be found in Table 5.1. If a measurement is done parallel to the X-direction with the $X+$ surface connected to the copper plate with positive potential, it is called $X+$. The opposite direction is called $X-$.

It can be seen that there is a difference between the various directions. The total resistance along the Z-direction is not getting higher than 1.03 mΩ. While the average resistance of the other directions is between 1.3 mΩ and 1.82 mΩ. It is also noticeable that the measurement methods themselves deviate too. The first measurement has the biggest deviation of 0.52 mΩ between the way of measuring.

For C2 the Z-intersection was measured via both methods to be between 0.6 mΩ and 0.7 mΩ. In contrast with the Y-intersection which was measured by both methods to be around 1.7 mΩ and 1.77 mΩ. Resulting in the total resistance being 1.1 mΩ lower along the Z-direction.

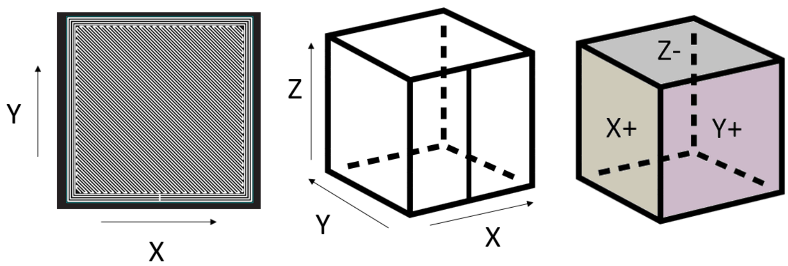

Figure 5.3: Figures showing how the 3D printed cubes measurement direction is defined. The Z-direction is the print direction. The left most figure is a top view of one layer of a cubic sample.

5.3 Discussion

5.3.1 External current source

A higher current results in a higher voltage drop over the sample. Consequently, the relative resolution of the meter improved compared to using the default 10 mA of the Agilent 34420A.

To prevent joule heating the external current source was limited to 200 mA. The larger cubic samples C1 and C2 can heat up by a maximum of $0.07\,\mu\mathrm{K\,s^{-1}}$ and the smaller samples C3 and C4 by a maximum of $1.13\,\mu\mathrm{K\,s^{-1}}$. The maximum heat forming per second is calculated using Equation 2.7 and assuming no heat is lost to the environment. Therefore creating a worst case scenario. A miscalculation led to the used current of 200 mA as a maximum, so more can be used. With a current of 10 A the temperature would rise with 2.82 $\mathrm{mK\,s^{-1}}$ for the C3 and C4 samples. Hence, these samples were not the bottleneck.

However, the copper wool was expected to heat up quicker as it has less weight and is made of small copper wires which increases resistance. This gave a larger temperature difference and, hence, imposed more thermoelectric voltage. The current source of the micro-ohm meter was not used during the voltage measurements. Therefore, offset compensation was not utilised and hence, the thermal EMF could have significant influence on the measurements.

5.3.2 Contact resistance

Using the micro-ohm meter of the Agilent 34420A the resistance of the cubes with contact resistance was first measured to be approximately 20 mΩ using a two-point measurement. The wires were attached the same as in the setup shown in Figure 5.1. The resistance of the copper plates was measured by holding the $V+$ and $V-$ probe on the plates, while not removing the current source. In the same manner this was done for the samples. This showed that both the plates and the sample individually were in the μΩ range. Therefore, it is supposed that the contact resistance contained the largest part of that resistance. To improve this copper wool was made from thin copper wire. This decreased the contact resistance significantly resulting in a total resistance of about 1.5 mΩ. To further lower the contact resistance a silver ink paste can be used. However, this was not implemented as the silver paste will harden which would inhibit further use of the measurement set up.

5.3.3 Anisotropy

The resistances along various directions of the cube were measured. A difference in resistance can indicate anisotropy. However, if that would be just 5% then that would mean for C3 and C4 a difference of 4.9 μΩ and for C1 and C2 not more than 2.45 μΩ. During sintering the metal particles fused together. As the sample shrank it was expected to contain less voids between the traces resulting in a more homogeneous material. In case of anisotropy a higher resistance was expected perpendicular to the printing path, because of voids along the printing path as was found in the analysis.

An anisotropic effect is found. However, this does not implicate that the anisotropic effect originates from the sample as well. As calculated in the methods section, the resistance of samples C1 and C2 is around 49 μΩ. That means the resistance change of 1 mΩ is approximately twenty times the resistance of the sample. The resistance of only the copper wool varies as well, while tightened it was measured to be 318 μΩ. However, when not tightened the resistance went up to more than 10 mΩ. As the measurements were unusable, further measurements with C2, C3 and C4 were not done.

The anisotropic effects also do not satisfy the results using the 3D model of Daniel Wilmes as stated in the analysis. There it was thought to be less conductive and thus would result in a higher resistance along the Z-direction. Due to the way of infill the X and Y-direction were assumed to be the same.

5.3.4 Meandering resistor anisotropy

Two types of meandering structures were fabricated, one with vertical meandering the other horizontal meandering respectively. Therefore, the print direction is changed and hence the influence on resistance could be investigated. The models can be seen in Figure 5.4. The original meandering wire has a total length of 221 mm, width of 0.5 mm and height of 0.5 mm. These width and height are chosen as the vertical meandering needs to create pillars that are still printable. Here the resistance is 866 mΩ, which is four times less then the horizontal one layer meandering version. If the 0.5 mm in diameter is not enough, then a 1 mm diameter for the

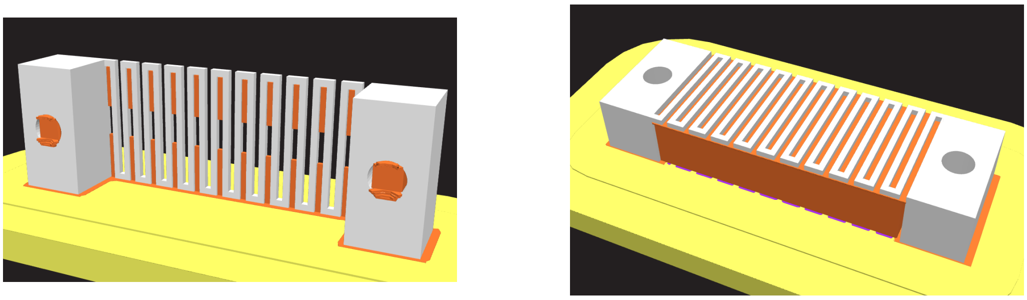

(a) The meandering resistor printed vertically.

(b) The meandering resistor printed horizontally.

Figure 5.4: Two specific samples for the meandering resistors.

pillars may be used, but that decreases the total resistance again by four, resulting in 217 mΩ. In the same space, the horizontal meandering can fit four layers of 3.47 Ω resulting in a total resistance of 13.88 Ω. This is approximately 64 times higher than the vertical meandering resistor with a diameter of 1 mm. Hence, designing bigger pillar diameters is not beneficial if the 0.5 mm diameter does not work. As the samples failed to print and sinter as was described in chapter 3 these experiments could not be done.

5.3.5 Plate anisotropy

It was taken into account that the cubes would have too little resistance to be measured accurately. Furthermore the pillars of the meandering design could be too unstable, and hence, the part would fail. Then another experiment using plates could help with finding the anisotropic parameters. There were two plates printed, with one being along the YZ-plane and the other in the XY-plane. These plates have higher resistance than the cubes, but are not as fragile as the meandering pillar. These plates could then be put in the setup in Figure 4.1. Alas, as the sintering went wrong, these samples were not available for anisotropy experiments.

5.4 Conclusion

Experiments were done to find anistropy in the sintered samples C1, C2 and C3. However, the measurements gave no useful results as the resolution that was needed could not be obtained. The contact resistance was significant and varied, meaning the setup did not work. The results also did not satisfy the model that was adjusted from Daniel Wilmes 3D model.

For further research, 3D printed plates could work better as they have a higher resistance.

6 Discussion

6.1 Printing problems

Inconsistencies in dimensions and electrical resistivity were encountered. Therefore, resistive sensors that are intended to be fabricated using the ADAM 3D metal printing technique need to undergo calibration. Calibration needs to be done on the resistance and on the resistive response on mechanical strain. The amount of work that it would take to calibrate a sensor should be investigated, but can be expected to be challenging as multiple factors play a role in the inaccuracies. In the example of the medical application with the plates for the fractured bones, the plate that supports the bone while rehabilitating may be exposed to different temperatures, especially in the limbs. This has an influence on the electrical resistance and is one of the expected problems for calibration.

6.2 Measuring small resistances

Even while using various setups and equipment the measurements were troublesome. The contact resistance should be below 1% to be so small that it can be neglected compared to the measured resistance. However, in the cases of the cubes they were 15 and 30 times the theoretical resistance of the cubes, taking in account the contact resistance of 1.5 mΩ.

The copper wool proved to be helpful in elimination of some contact resistance for the cubes lowering it from 20 mΩ to approximately 1.5 mΩ. However, the contact resistance for the wires could not be lowered as the copper wool could not be made to make more contact point with the copper plates.

The resistance of the wires itself was high enough to still perform measurements. The contact resistance fluctuated and was of magnitudes that it could not be neglected. When dealing with small resistance measurements, factors that normally can be neglected play a significant role for these cases. Examples can be temperature fluctuations, force on the contacts, fluctuations in the designed dimension, materials, type of measurement wires, measuring techniques. Using a sensor which measures small resistances is difficult to make accurate, due to the many influences which cause fluctuations in the readings. Hence it is difficult to make a feasible sensor design out of only one single piece of conductive material.

6.3 Contact resistance

6.3.1 Thermoelectric voltages

The micro-ohm meter with a four-point measurement was used for most measurements. With a four-point measurement there are four connections that all can create thermoelectric voltages and hence it was expected to have a significant influence. The Seebeck coefficient of 17-4PH stainless steel was not found nor calculated. However, 17-4PH stainless steel contains nickel, copper and mainly iron. Iron has a Seebeck coefficient of $19\,\mu VK^{-1}$ at 0 °C [37]. It is decreasing approximately linearly with the material's temperature as can be seen in Figure 6.1. Subtracting the copper coefficient from iron a Seebeck coefficient of $12.5\,\mu VK^{-1}$ is obtained.

If it would be only iron, that would mean that for every degree, a resistance change of 1.25 mΩ would be measured, per contact for the current of 10 mA applied by the Agilent. As this is in the range of the measurements it would be problematic.

However, the micro-ohm meter has an offset compensation which was used during all measurements. For a sensor which measures small resistances and is not made out of one material, this can be a useful technique to implement as well. It also shows a benefit of making the sensor out of a single metal structure to prevent creating thermoelectric voltages.

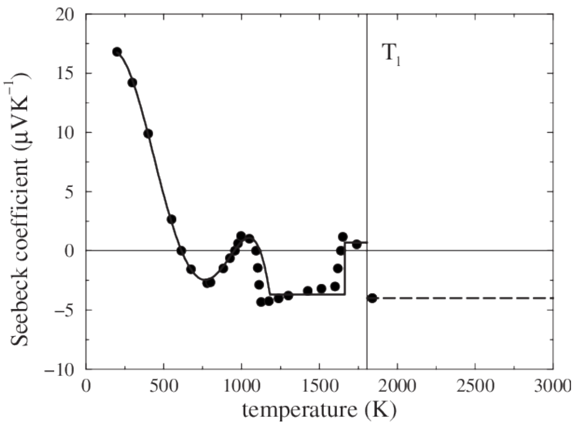

Figure 6.1: "Seebeck coefficient of iron Fe versus the temperature T." Adapted from [38].

6.3.2 External current source

A way to improve the measurement was increasing the current using an external current source. However, this was done by limiting the current rather than accurately define the current output. The current coming out of the external current meter was measured using a handheld multimeter. The external current was a factor of approximately 0.5 of on what the external current source stated. Hence, these measurements can still be improved by using a source measurement unit (SMU) that can accurately output a stable current. However, an SMU was not available at the time of the research.

6.4 Anisotropy

Changing the cube so that the $Z+$ and $Z-$ surfaces were connected to the copper wool and copper plates made the total resistance 30% up to more than 50% lower. As that is a larger fluctuation than for the whole resistance that the cubes should have this possibly is not only an anisotropic effect of the material. It is likely that the effects of the contact resistance of the different surfaces is measured. The bottom of the sample had voids between the lines of leaked steel. If the copper wool got right in those voids it could possibly make much better contacts, eliminating a large portion of the contact resistance. As the plates nor the meandering resistors came out of the printing process unharmed the anisotropic effect could not be tested.

The anisotropic effect is important when it has a lot of influence as the sensor needs to be designed in specific geometrical orientations to still achieve accurate resistances. The anisotropic effect on the conductive thermoplastic composites acrylonitrile butadiene styrene copolymer (ABS) and carbon black (CB) was investigated. This showed that the resistivity in the vertical direction ranged from 70 Ωm to 180 Ωm while the horizontal direction had a resistivity of 42 Ωm to 58 Ωm [39]. These values are significantly different. For the metal part this will not be the case. Compared to the conductive thermoplastic composites the metal will be rather isotropic as the resistance changes in the μΩcm to maybe mΩcm range, instead of 28 mΩcm to 122 mΩcm.

6.5 Titanium

Although stainless steel is at the moment also widely used for medical applications, it is interesting to see what other materials could be better suited for electrical and biomechanical solutions. An example which can be seen in the datasheet from the Markforged Metal X printer is that they offer Titanium Ti-6Al-4V as printing material [40]. After searching about details, it is clear that Markforged does not offer it anymore and even removed it from the new version of the datasheet. However, as the stainless steel is not easily used for resistive sensors, the titanium alloy offers better properties. The bulk material has for example an electrical resistivity of 178 µΩ cm, which is more than twice as high as that of 17-4PH stainless steel [41]. Next to that it has an elongation at break of 10%, compared to 5% of stainless steel and a modulus of elasticity of 114 GPa which is around 60 GPa less [41]. So, next to being able to create isolated parts in the material easier, due to the higher electrical resistivity, making resistive sensors like a strain gauge is also better, making the resolution bigger due to better elasticity. As it is also a good biocompatible material this is a more suitable solution for the metal plates to help support fractured bones. When Markforged makes this material printable then further investigation of resistive sensors in Ti-6Al-4V is recommended.

7 Recommendations

Several recommendations for future research were made. In this chapter they are listed in a short overview.

- Further research into 3D printed metal sensors could be to test the ceramic more. The ceramic can be chosen to replace two extra layers of metal support instead of all, making the total height of the ceramic 0.5 mm instead of the default 0.25 mm. It is interesting to see if the metal would then still leak through or that it is enough and that the metal support can also be easily removed. Also interesting to see is if this will still induce problems during sintering resulting in a failed end product.
- The settings for the furnace could be changed to see if parts can be partially sintered. Therefore, using the parts that are not completely fused as insulation material.
- As some parts were more fragile than others it is expected that the salvaged samples were not equally sintered. Further research could investigate this.
- To further lower the contact resistance a silver ink paste can be used. However, this could inhibit further use of the measurement set up as it can harden.
- For future measurements on the anisotropic properties various thin samples in the form of plates could be used better than cubic samples.
- If resistive sensors are build, it is recommended to use thermoelectric offset compensation for measurements.
- It can be interesting to see if other metals, like titanium, can be better used to fabricate resistive sensors.

8 Conclusion

Integrated sensing functionality was investigated with metal 3D printed 17-4PH stainless steel. First the mechanical and electrical properties were researched. As more was known about the mechanical properties, the electrical properties were mainly investigated. Due to the resistance being in $\mu\Omega$ or $m\Omega$ range, finding the right measurement setup and techniques was difficult. Therefore, several different setups were made. The electrical resistivity was finally found to be fluctuating around -5% to +6% from the theoretical resistivity of $98\,\mu\Omega$. These measurements were done over a salvaged piece of wire of 1 cm and a meander of 1.8 cm. The contact resistance of these samples were measured and was fluctuating for every sample in the $m\Omega$ range. The measurements that were done before this setup was used had higher fluctuations in electrical resistivity. An anisotropic effect was found, but is probably caused by the contact resistance rather than the printed material itself. The anisotropic effect is relatively very small compared to e.g. TPU's and practically the material can be assumed to be isotropic for designing.

A magnetic sensor idea was found to be already working with another material. Another research could investigate if this could work with 17-4PH stainless steel as well considering that it is magnetic. To make a conductive sensor it was first needed to see if the various parts could be isolated well. Otherwise examples exist already with post processing using insulation materials. These measurements could not be done due to the failed test samples. Therefore, this research can provide no information on the integration of magnetic sensors and further research needs to be conducted in order to answer this question.

A meandering resistor with a volume of $2\,cm^3$ resulted in a theoretical resistance of $122.62\,\Omega$. It is expected that different metal parts can be isolated using these meandering resistors. However, printing limitations decrease this maximum resistance as the layers of metal meandering need to be further apart than one layer to prevent leaking. The exact number of ceramic layers between metal parts to prevent leaking and the use of full ceramic replacement of the metal support parts need to be further investigated. In the end it proved difficult to make a resistive sensor design due to inconsistencies in dimension and the low resistance and resistance changes. Hence, further research is needed, especially when the technology can also print better materials like titanium.

A Appendix

A.1 Figures

Figure A.1: A picture of the nozzles used by the Metal X system. Left is the nozzle for metal filament. Right is the nozzle for ceramic filament. Adapted from the Markforged webstore [42].

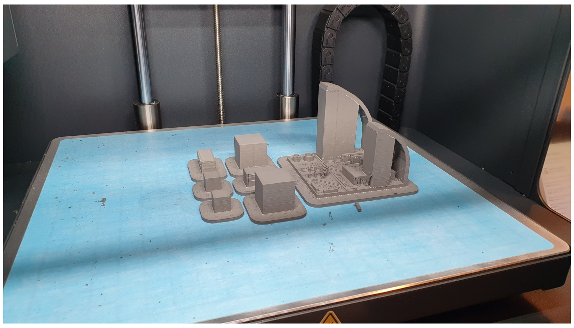

Figure A.2: A picture of the first round of samples that were printed. Here they can be seen in the printer. The big right structure is the calibration model.

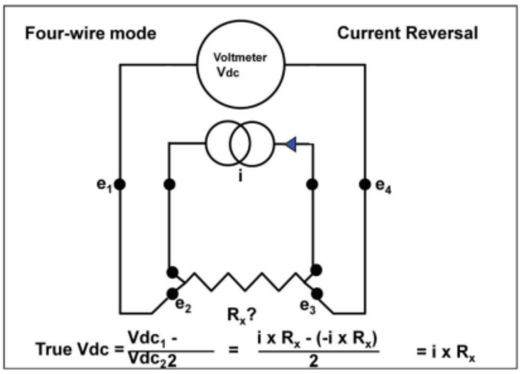

Figure A.3: A setup showing how two measurements are made with reversed current and are averaged to eliminate the thermoelectric voltage. Adapted from [43].

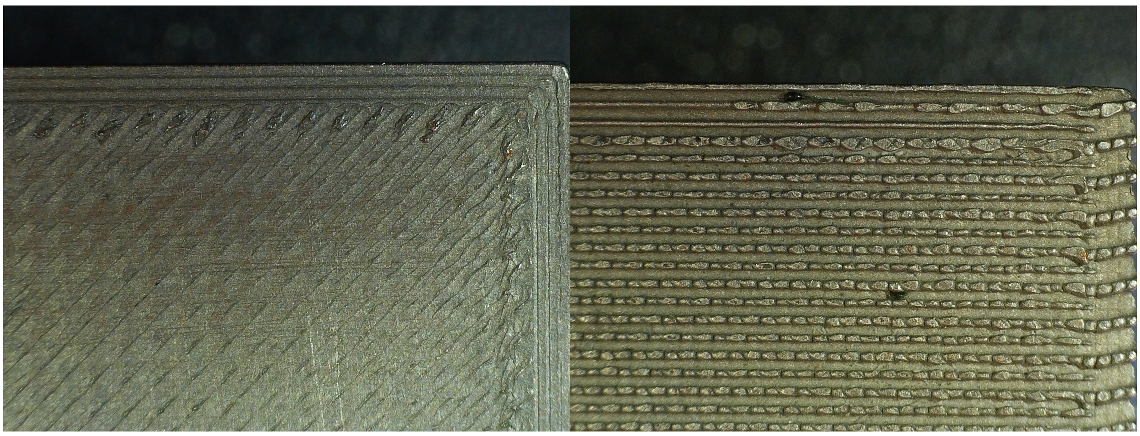

(a) A microscopic top view of sample C1.

(b) A microscopic bottom view of sample C1.

Figure A.4: Two pictures taken by a microscope of the top and bottom of a metal printed cube. The bottom has some leaked metal lines, while the top is smooth.

(a) Sample W1 with a length of 1 cm

(b) Salvaged meander wire sample M1 attached to the test setup.

Figure A.5: Two pictures showing sample W1 and M1.

A.2 Matlab code

A.2.1 Agilent 34420A measurements

```
clear all;

    OhmMeter = GPIB_34420A_init(27);
    fprintf(OhmMeter, '*rst'); %Reset
    fprintf(OhmMeter, 'conf:fres'); %Select configuration four point
 resistance measurement.
    fprintf(OhmMeter, 'sense:fres:range 10'); %Range min does not
 work.
    fprintf(OhmMeter, 'sense:fres:res min'); %Resolution is preferred
 to be minimal.
    fprintf(OhmMeter, 'sense:fres:ocom on'); %Offset compensation on.
    fprintf(OhmMeter, 'sense:fres:nplc 20'); %Due to time constraint
 the test is integrated over 20 cycles.
        fprintf(OhmMeter, 'OUTPut:STATe?'); %Ask the output state.
        state = fscanf(OhmMeter); %Get the result of the output state.

tic

for i=1:25
    fprintf(OhmMeter, 'sense:fres:ocom?'); %Ask the state of the
 offset compensation.
    rawoff = fscanf(OhmMeter); %Get the result of the state.
    offset_compensation(i) = str2num(rawoff); %Put the results per
 measurement in a table.
    fprintf(OhmMeter, 'sense:fres:nplc?'); %Ask the state for the
 integrated cycles.
    rawnplc = fscanf(OhmMeter); %Get the result of the state.
    nplcstatus(i) = str2num(rawnplc); %Put the results per measurement
 in a table.
    fprintf(OhmMeter, 'read?'); %Do a measurement.
    rawStr = fscanf(OhmMeter); %Get the measurement.
    data(i) = str2num(rawStr) %Put the measurement in a table.
    toc
end
```

Published with MATLAB® R2020b

1

Figure A.6: Code for the readings using Agilent 34420A and Matlab.

A.2.2 Least mean square curve fitting

Least mean square fitting

First create two variables. Data are the measured values and x is the horizontal axis.

```
y = data;
X = [ones(size(x)); x];
Y = y;

theta = Y*pinv(X); % Multiplying the measurements with the Moore-
Penrose Pseudoinverse of matrix X.
f = @(x) theta(1) + theta(2)*x;
xx = linspace(0, 17, 500);
yy = f(xx);

figure;
plot(xM,y,'Or', 'DisplayName', 'Data Points');
hold on;
plot(xx, yy,'b', 'DisplayName', 'Curve fit');
xlabel('Distance [mm]');
ylabel('Resistance [Ohm]');
grid on;
legend show;
```

Published with MATLAB® R2020b

1

Figure A.7: Code for the least mean square curve fitting of the resistance over length measurements. Adapted from Mostapha Kalami Heris on his Youtube channel [44].

Bibliography

[1] AGS Health in Aging Foundation, "Fractures," 2020, accessed: 28.04.2022. [Online]. Available: https://www.healthinaging.org/a-z-topic/fractures/basic-facts

[2] I. H. Kalfas, "Principles of bone healing," *Neurosurgical Focus*, vol. 10, no. 4, pp. 1–4, 2001. [Online]. Available: https://doi.org/10.3171/foc.2001.10.4.2

[3] All3DP, "10 best ways to 3d print metal," 2022, accessed: 30.03.2022. [Online]. Available: https://all3dp.com/1/best-ways-to-3d-print-metal/?utm_source=newsletter&utm_medium=email&omhide=true

[4] M. Schouten et al., "A review of extrusion-based 3d printing for the fabrication of electro- and biomechanical sensors," *IEEE Sensors Journal*, vol. 21, no. 11, pp. 12 900–12 912, 2021.

[5] M. Ahart, "Types of 3d printing technology," 2019, accessed: 30.03.2022. [Online]. Available: https://www.protolabs.com/resources/blog/types-of-3d-printing/

[6] A. B. Varotsis, "Introduction to binder jetting 3d printing," 2021, accessed: 30.03.2022. [Online]. Available: https://www.hubs.com/knowledge-base/introduction-binder-jetting-3d-printing/#what

[7] AMFG Autonomous Manufacturing, "Metal 3d printing: Where are we today?" 2019, accessed: 30.03.2022. [Online]. Available: https://amfg.ai/2019/02/19/metal-3d-printing-where-are-we-today/#:~:text=The%20origins%20of%20direct%20metal,laser%20sintering%20(DMLS)%20technology.

[8] Markforged, "Material datasheet 17-4 ph stainless steel," 2020, accessed: 14.02.2022. [Online]. Available: https://www-objects.markforged.com/craft/materials/17-4-V2.1.pdf

[9] ——, "Material datasheet composites," 2021, accessed: 14.02.2022. [Online]. Available: http://static.markforged.com/downloads/composites-data-sheet.pdf

[10] ——, "The markforged metal additive manufacturing process," 2019, accessed: 14.02.2022. [Online]. Available: https://markforged.com/jp/resources/learn/design-for-additive-manufacturing-metals/metal-additive-manufacturing-introduction/metal-additive-manufacturing-process

[11] ——, "Eiger," 2022, accessed: 28.04.2022. [Online]. Available: https://www.eiger.io/

[12] M. Galati et al., "Analysis of density, roughness, and accuracy of the atomic diffusion additive manufacturing (adam) process for metal parts," *Materials (Basel)*, vol. 12, no. 24, 2019. [Online]. Available: https://doi.org/10.3390/ma12244122

[13] F. IJpma, "Personal conversation on 10.03.2022."

[14] Y. Tan et al., "A passive and wireless sensor for bone plate strain monitoring," *Sensors*, vol. 17, no. 11, 2017. [Online]. Available: https://doi.org/10.3390/s17112635

[15] A. Hehr, "Print metal parts with built-in sensors," 2018, accessed: 01.04.2022. [Online]. Available: https://www.machinedesign.com/3d-printing-cad/article/21836455/print-metal-parts-with-builtin-sensors

[16] V. Zega et al., "A 3d printed ti6al4v alloy uniaxial capacitive accelerometer," *IEEE Sensors Journal*, vol. 21, no. 18, pp. 19 640 – 19 646, 2021. [Online]. Available: https://doi.org/10.1109/JSEN.2021.3095760

[17] Tech Steel & Materials, "Stainless steel 17-4ph," 2022, accessed: 28.04.2022. [Online]. Available: https://www.techsteel.net/alloy/stainless-steel/17-4ph

[18] J. Haworth, "The markforged metal x: An introduction to metal 3d printing," 2019, accessed: 14.02.2022. [Online]. Available: https://hawkridgesys.com/blog/the-markforged-metal-x-an-introduction-to-metal-3d-printing

[19] H. Kwan, "Resistivity of nichrome," 2007, accessed 10.03.2022. [Online]. Available: https://hypertextbook.com/facts/2007/HarveyKwan.shtml

[20] Metal Supermarkets, "Is stainless steel magnetic?" 2018, accessed: 28.04.2022. [Online]. Available: https://www.metalsupermarkets.com/is-stainless-steel-magnetic/#:~:text=The%20unique%20crystal%20structure%20of,many%20martensitic%20stainless%20steels%20magnetic.

[21] T.C. Henry et al., "Mechanical behavior of 17-4 ph stainless steel processed by atomic diffusion additive manufacturing," *The International Journal of Advanced Manufacturing Technology. 114*, pp. 2103–2114, 2021. [Online]. Available: https://link.springer.com/article/10.1007/s00170-021-06785-1

[22] D. Wilmes, "Modelling, characterization and visualization of anisotropic electrical behaviour in cuboids of fused-deposition-modelling 3d prints," Individual project, University of Twente, 2021.

[23] C. Perabo, "Volume resistivity vs. volume conductivity vs. surface resistivity," 2013, accessed: 28.04.2022. [Online]. Available: https://www.caplinq.com/blog/linqstat-volume-resistivity-vs-volume-conductivity-vs-surface-resistivity_267/

[24] A. Dijkshoorn et al., "Characterizing the anisotropic electrical properties of 3d printed conductive sheets," Master's Thesis, University of Twente, 2019.

[25] J. Lourtioz et al., *Photonic Crystals: Towards Nanoscale Photonic Devices*, 2nd ed. Heidelberg, Germany: Springer, 2008. [Online]. Available: https://doi.org/10.1007/978-3-540-78347-3

[26] Markforged, "Design guide for 3d printing with metals version 1.6," 2022, accessed: 14.02.2022.

[27] J. Daniels, "Strain gauges," 2014, accessed: 10.03.2022. [Online]. Available: https://www.brown.edu/Departments/Engineering/Courses/En123/Lectures/StrainFromCyber.htm

[28] Osilla.com, "Sheet resistance measurements of thin films," 2018, accessed: 14.02.2022. [Online]. Available: https://www.ossila.com/en-eu/pages/sheet-resistance-measurements-thin-films

[29] M. Sophocleous et al., "Electrical resistivity sensing methods and implications," in *Electrical Resistivity and Conductivity.* London, United Kingdom: IntechOpen, 2017, ch. 2. [Online]. Available: https://doi.org/10.5772/67748

[30] R. Menezes, "How to convert wattage to degrees," 2017, accessed: 28.04.2022. [Online]. Available: https://sciencing.com/how-8174875-calculate-btu-heat.html

[31] Engineering ToolBox, "Specific heat of common substances." 2003, accessed: 28.04.2022. [Online]. Available: https://www.engineeringtoolbox.com/specific-heat-capacity-d_391.html

[32] Agilent Technologies, “Agilent 34420a nano volt / micro ohm meter user’s guide,” 2021, accessed: 10.03.2022. [Online]. Available: http://instructor.physics.lsa.umich.edu/adv-labs/Tools_Resources/HP%2034420A%20user’s%20guide.pdf

[33] Dassault Systèmes, “Solidworks,” 2022, accessed: 28.04.2022. [Online]. Available: https://www.solidworks.com/

[34] RS PRO, “datasheet rs pro electronic digital caliper 150mm/6,” 2019, accessed: 10.03.2022. [Online]. Available: https://docs.rs-online.com/9422/0900766b813d64f6.pdf

[35] Eleshop.nl, “Rohde & schwarz hm8118 lcr meter,” 2022, accessed: 10.03.2022. [Online]. Available: https://www.eleshop.nl/rohde-schwarz-hm8118-lcr-meter.html

[36] Farnell, “Skytronic 650.682 instruction manual,” 2014, accessed: 28.04.2022. [Online]. Available: https://www.farnell.com/datasheets/29426.pdf

[37] A. Molki, “Simple demonstration of the seebeck effect,” 2010, accessed: 28.04.2022. [Online]. Available: https://files.eric.ed.gov/fulltext/EJ925482.pdf

[38] A. Lange et al., “Thermoelectric currents in laser induced melts pools,” *Journal of Laser Applications VOL. 21, NO. 2*, 2009, accessed: 28.04.2022.

[39] J. Zhang et al., “Resistivity and its anisotropy characterization of 3d-printed acrylonitrile butadiene styrene copolymer (abs)/carbon black (cb) composites,” *Applied Science*, vol. 7, no. 1, 2017. [Online]. Available: https://doi.org/10.3390/app7010020

[40] Markforged, “Product specificatoins: Metal x,” 2020, accessed: 14.02.2022. [Online]. Available: https://3dtechnology.ie/wp-content/uploads/2020/12/Metal_System_Datasheets.pdf

[41] Matweb, “Titanium ti-6al-4v (grade 5), annealed bar,” 2022, accessed: 30.03.2022. [Online]. Available: https://www.matweb.com/search/datasheet_print.aspx?matguid=10d463eb3d3d4ff48fc57e0ad1037434

[42] Markforged, “Metal x nozzle pack,” 2018, accessed: 30.03.2022. [Online]. Available: https://www.mark3d.com/en/product/markforged-metal-consumables/metal-x-nozzle-pack/

[43] M. L. Kidd, “Watch out for those thermoelectric voltages!” 2012, accessed: 30.03.2022. [Online]. Available: https://www.google.com/url?sa=i&url=https%3A%2F%2Fdownload.flukecal.com%2Fpub%2Fliterature%2Fp18-21.pdf&psig=AOvVaw3JrzW83_Pc_k9vQu20uUvO&ust=1654249255338000&source=images&cd=vfe&ved=0CAwQjRxqFwoTCNjMgO28jvgCFQAAAAAdAAAAABAJ

[44] M. K. Heris, “Least squares: Theory and implementation using matlab, python and javascript,” 2019, accessed: 28.04.2022. [Online]. Available: https://www.youtube.com/watch?v=pf6BHN0IFaY&ab_channel=Yarpiz